

Screening Mixed-Metal $\text{Sn}_2\text{M(III)Ch}_2\text{X}_3$ Chalcohalides for Photovoltaic Applications

Pascal Henkel,[†] Jingrui Li,[‡] G. Krishnamurthy Grandhi,[¶] Paola Vivo,[¶] and Patrick
Rinke*,[†]

[†]*Department of Applied Physics, Aalto University, P.O.Box 11100, FI-00076 AALTO,
Finland*

[‡]*Electronic Materials Research Laboratory, Key Laboratory of the Ministry of Education
and International Center for Dielectric Research, School of Electronic Science and
Engineering & International Joint Laboratory for Micro/Nano Manufacturing and
Measurement Technology, Xi'an Jiaotong University, Xi'an 710049, China*

[¶]*Hybrid Solar Cells, Faculty of Engineering and Natural Sciences, Tampere University,
P.O. Box 541, Tampere, FI, 33014, Finland*

E-mail: patrick.rinke@aalto.fi

Abstract

Quaternary mixed-metal chalcohalides ($\text{Sn}_2\text{M(III)Ch}_2\text{X}_3$) are emerging as promising lead-free perovskite-inspired photovoltaic absorbers. Motivated by recent developments of a first $\text{Sn}_2\text{SbS}_2\text{I}_3$ -based device, we used density functional theory to identify lead-free $\text{Sn}_2\text{M(III)Ch}_2\text{X}_3$ materials that are structurally and energetically stable within $Cmcm$, $Cmc2_1$ and $P2_1/c$ space groups and have a band gap in the range of 0.7–2.0 eV to cover out- and indoor photovoltaic applications. A total of 27 $\text{Sn}_2\text{M(III)Ch}_2\text{X}_3$ materials were studied, including Sb, Bi, In for M(III)-site, S, Se, Te for Ch-site and Cl, Br, I for X-site. We identified 12 materials with a direct band gap that meet our requirements,

namely: $\text{Sn}_2\text{InS}_2\text{Br}_3$, $\text{Sn}_2\text{InS}_2\text{I}_3$, $\text{Sn}_2\text{InSe}_2\text{Cl}_3$, $\text{Sn}_2\text{InSe}_2\text{Br}_3$, $\text{Sn}_2\text{InTe}_2\text{Br}_3$, $\text{Sn}_2\text{InTe}_2\text{Cl}_3$, $\text{Sn}_2\text{SbS}_2\text{I}_3$, $\text{Sn}_2\text{SbSe}_2\text{Cl}_3$, $\text{Sn}_2\text{SbSe}_2\text{I}_3$, $\text{Sn}_2\text{SbTe}_2\text{Cl}_3$, $\text{Sn}_2\text{BiS}_2\text{I}_3$ and $\text{Sn}_2\text{BiTe}_2\text{Cl}_3$. A database scan reveals that 9 out of 12 are new compositions. For all 27 materials, $P2_1/c$ is the thermodynamically preferred structure, followed by $Cmc2_1$. In $Cmcm$ and $Cmc2_1$ mainly direct gaps occur, whereas mostly indirects in $P2_1/c$. To open up the possibility of band gap tuning in the future, we identified 12 promising $\text{Sn}_2\text{M(III)}_{1-a}\text{M(III)'}_a\text{Ch}_{2-b}\text{Ch}'_b\text{X}_{3-c}\text{X}'_c$ alloys which fulfill our requirements and additional 69 materials by combining direct and indirect band gap compounds.

1 Introduction

Photovoltaic technologies are instrumental for the transition from conventional to green and renewable energy production. To increase the power conversion efficiency while reducing costs and improving device longevity, new materials are continuously being explored. Lead halide perovskites (LHPs) have emerged as promising contenders due to their beneficial optoelectronic properties, defect-tolerance, and cost-effective solution processing. Yet, the toxicity of lead and the moderate long-term stability in air¹⁻⁴ impede the commercial viability of LHPs. Sn^{2+} -based perovskites and Sb^{3+} - and Bi^{3+} -based perovskite-inspired absorbers are popular low-toxicity alternatives, but suffer from air-oxidation (Sn^{2+} to Sn^{4+})⁵ and high defect densities.^{6,7} Conversely, metal chalcogenides (e.g., Pb-, Cd-, Sb-based)⁸⁻¹⁰ with tunable band gaps and high absorption cross-sections have enabled highly stable solar cells with modest efficiencies. Mixed-metal chalcogenides with $\text{M(II)}_2\text{M(III)Ch}_2\text{X}_3$ stoichiometry (also referred to as $\text{A}_2\text{BCh}_2\text{X}_3$)¹¹ are an emerging semiconductor family combining halide perovskite and metal chalcogenide building blocks.¹¹⁻¹³ The Ch-sites are occupied by the bivalent chalcogenide anions that form strong metal-chalcogen bonds with the metal cations. Mixed-metal chalcogenides may display the intriguing optoelectronic properties of LHPs, such as the dispersive valence and conduction bands, the high defect tolerance due to strong dielectric screening (owing to the presence of ns^2 lone pair cations) and the resultant low capture

cross-sections of defects,^{1,2,12} with the promise to overcome the pressing stability challenges of LHPs.^{4,12} In addition, the Sn-Ch bonding nature should prevent the Sn²⁺ to Sn⁴⁺ oxidation in mixed-metal chalcogenides. Also, experimental X-ray photoelectron spectroscopy measurements suggest that synthesizing Sn₂M(III)Ch₂X₃ under reduction conditions partly suppresses Sn²⁺ to Sn⁴⁺ oxidation.¹² As a result, Sn₂M(III)Ch₂X₃ films are stable even in humid environments.^{11,12} The photovoltaic potential of mixed-metal chalcogenides was recently demonstrated for a Sn₂SbS₂I₃-based single-junction solar cell that achieved a power conversion efficiency (PCE) of 4.04%.¹² This is a promising start considering that the first perovskite solar cells only reached a PCE of 3.8% in 2009¹⁴ and now exceed 25%.¹⁵

Over the past four decades the M(II)₂M(III)Ch₂X₃ material space – lead-free as well as the lead-based - has only scarcely been explored (both theoretically and experimentally) and only a few compounds are known such as Sn₂SbS₂I₃,^{11,12,16,17} Sn₂SbSe₂I₃,¹⁸ Sn₂BiS₂I₃,¹⁹ Pb₂SbS₂I₃^{20–22} and Pb₂BiS₂I₃.^{19,22} X-ray diffraction (XRD) revealed that M(II)₂M(III)Ch₂X₃ materials crystallize predominantly in an orthorhombic *Cmcm* space group.^{16,18–22} For Sn₂SbS₂I₃, density functional theory (DFT) calculations demonstrated that this *Cmcm* structure has to be interpreted as an average over energetically more favorable, lower symmetry *Cmc2₁* configurations.¹¹ XRD measurements by Doussier *et al.* further found that Pb₂SbS₂I₃ changes to a monoclinic *P2₁/c* structure below 100 K.²¹ This *P2₁/c* structure was then shown to be lower in energy than the *Cmcm* and *Cmc2₁* phases for Sn₂SbS₂I₃ by DFT.¹⁷ In addition, for Sn₂SbS₂I₃, UV-vis absorption spectroscopy and DFT calculations revealed that the optical band gap lies below 1.5 eV.^{11,12,23} This limits its applications to single-junction solar cells as the band gap is close to the optimum value of harvesting solar radiation (1.3 eV).^{24,25} In contrast, materials with a wide-band gap (1.6–2.5 eV) will be of interest for emerging applications such as indoor and tandem photovoltaics.²⁶

Materials exploration can facilitate materials discovery for targeted properties and we apply it here to look for promising Sn₂M(III)Ch₂X₃ materials. By now, many materials databases have been compiled²⁷ and one could search them for materials that meet speci-

fied design criteria.^{28–30} Materials or compounds that are not expected to be cataloged in databases can be explored by means of high-throughput computational or synthesis methods, often aided by machine-learning.^{31–36} Higher dimensional spaces offered by, e.g., quaternary or quinary materials still pose challenges, however, due to their sheer size and complexity. Such high-dimensional materials spaces have therefore only been explored partially.

We here add an exploration of a $\text{Sn}_2\text{M(III)Ch}_2\text{X}_3$ quaternary and quinary sub space for lead-free photovoltaic devices, which is chosen such that it can still be explored with DFT. For the M(III)-site, we considered both Sb^{3+} and Bi^{3+} (ns^2 lone pair), and In(III) (with ns^0 (d^{10}) valence electron configuration). The chalcogen (Ch) site is populated by S^{2-} , Se^{2-} or Te^{2-} , and the halogen (X) sites by Cl^- , Br^- or I^- , which yields altogether 27 materials. We furthermore accounted for structural diversity by including the three reported space groups ($Cmcm$, $Cmc2_1$, and $P2_1/c$).

For each material and each phase, we carried out DFT calculations within the generalized gradient approximation to assess structural stability and with a hybrid functional to quantify the electronic structure. We then screened for thermodynamic stability and suitable band gap. Promising material candidates are cross-checked against a variety of databases and datasets to assess their novelty. Lastly, we investigated the potential to tailor the band gap by exploring different $\text{Sn}_2\text{M(III)}_{1-a}\text{M(III)'}_a\text{Ch}_{2-b}\text{Ch}'_b\text{X}_{3-c}\text{X}'_c$ alloys.

The outline of this manuscript is as follows: In section II we describe our computational workflow including the screening criteria and the material cross-check. In Section III, we present and discuss our results for promising $\text{Sn}_2\text{M(III)Ch}_2\text{X}_3$ materials, as well as for $\text{Sn}_2\text{M(III)}_{1-a}\text{M(III)'}_a\text{Ch}_{2-b}\text{Ch}'_b\text{X}_{3-c}\text{X}'_c$ alloys. We conclude with a summary in Section IV.

2 Computational Details

2.1 Density-functional theory calculations

We performed periodic, spin unpolarized DFT calculations with the all-electron, numeric atom-centered orbital code FHI-AIMS³⁷⁻⁴². For exchange and correlation (XC), we used the Perdew-Burke-Ernzerhof functional for solids (PBEsol)^{43,44}, which provides good agreement with experiment for the lattice constants of various halide perovskites at reasonable computational cost.⁴⁵⁻⁴⁷ The atomic structure was relaxed with the Broyden-Fletcher-Goldfarb-Shanno algorithm and analytical stress tensor.⁴⁸ Every structure was pre-optimized using *light* real-space grid setting with a tier-1 basis set and was refined with *tight* settings and a tier-2 basis set. We applied a Gaussian broadening of 0.01 eV to the electronic occupations and relativistic effects were considered based on the zero-order regular approximation.^{37,49} The convergence threshold for the electronic self-consistency was set to 1×10^{-6} eV. The $\text{Sn}_2\text{M(III)Ch}_2\text{X}_3$ structures were relaxed until all forces acting on the atoms were smaller than 5×10^{-3} eV \AA^{-1} . Following the structural optimisations with PBEsol, we performed single point calculations for the band structure, the band gap, and the absorption spectra with the range-separated hybrid Heyd-Scuseria-Ernzerhof (HSE06) XC functional (with 25% exact exchange)⁵⁰⁻⁵², spin orbit coupling⁵³ and also a tier-2 basis. The latter were calculated on the basis of the linear macroscopic dielectric tensor⁵⁴ within the independent particle approximation.

We calculated each material in three crystal structures. For the #63/*Cmcm* (see Figure 1a)) and #36/*Cmc2₁* (see Figure 1b)) phases we used 16 atom unit cells and for the #14/*P2₁/c* (see Figure 1c)) phase a 32 atom unit cell. In Sec. 2.2 below, we describe the three crystal structures of *Cmcm*, *Cmc2₁* and *P2₁/c* in more detail. A Γ -centered k -point mesh was used for both PBEsol and HSE06 calculations. For the atomic structure relaxation with PBEsol, we used a Γ -centered $11 \times 11 \times 3$ k -point mesh for the *Cmcm* and *Cmc2₁* phases and a $6 \times 3 \times 5$ for *P2₁/c*. The HSE band structure calculations we performed with

Γ -centered $16 \times 16 \times 4$ for $Cmcm$ and $Cmc2_1$ and $9 \times 4 \times 8$ for $P2_1/c$.

To estimate the thermodynamic stability (at 0 K) we calculated the formation energy with respect to elemental decomposition of an individual $\text{Sn}_2\text{M(III)Ch}_2\text{X}_3$ material as

$$E_{\text{form}}(\text{Sn}_2\text{M(III)Ch}_2\text{X}_3) = E_{\text{tot}}(\text{Sn}_2\text{M(III)Ch}_2\text{X}_3) - \sum_i x_i \mu_i. \quad (1)$$

$E_{\text{tot}}(\text{Sn}_2\text{M(III)Ch}_2\text{X}_3)$ denotes the (DFT-calculated) total energy of $\text{Sn}_2\text{M(III)Ch}_2\text{X}_3$, μ_i the chemical of the i th element and x_i the corresponding number of atoms. The upper limit for the chemical potential is given by $\mu_i \leq E_{\text{tot}}(i\text{th element})$, i.e., the total energy per atom in the most stable phase of the i th element.⁵⁵ We used the following elemental compounds applying analogous computational parameters (with adjusted Γ -centered k -point mesh): Sb $R\bar{3}m$ (#166), Bi $R\bar{3}m$ (#166), In $I4/mmm$ (#139), S $Fddd$ (#70), Se $P2_1/c$ (#14) and Te $P3_121$ (#152), as well as Cl, Br and I in the gas phase as X_2 .

In the interest of open materials science²⁷, all relevant data is publicly available 10.17172/NOMAD/2023.08.24-1

2.2 $\text{Sn}_2\text{M(III)Ch}_2\text{X}_3$ structures

$\text{Sn}_2\text{M(III)Ch}_2\text{X}_3$ has been reported in three different space groups: $Cmcm$, $Cmc2_1$, and $P2_1/c$ (see Figure 1). In the $Cmcm$ phase SnCh_3X_2 pyramids share edges and form periodically continued $[\text{Sn}_2\text{Ch}_2\text{X}_2]_n$ chains along the a axis. The 1D $[\text{Sn}_2\text{Ch}_2\text{X}_2]_n$ chains in $\text{Sn}_2\text{M(III)Ch}_2\text{X}_3$ $Cmcm$ are connected by a M(III)X unit along the c axis to form a 2D $\text{Sn}_2\text{M(III)Ch}_2\text{X}_3$ structure within the ac plane. These 2D planes are not connected by chemical bonds along the b axis (see Figure 1 a)). In $Cmc2_1$ (Figure 1 b)), the M(III)X element exclusively bonds to a single $[\text{Sn}_2\text{Ch}_2\text{X}_2]_n$ chain, forming a periodically linked $[\text{Sn}_2\text{M(III)Ch}_2\text{X}_3]_n$ chain along the a axis, while the periodic connection along the c axis is interrupted. Analogous to $Cmcm$, no linking is present along the b axis. The asymmetric location of M(III) between the chains (i.e., different to $Cmcm$) results in a reduction of every

second square pyramidal SnCh_2X_3 polyhedron to an AX_3 tetrahedron, while simultaneously forming an additional square pyramidal SnChX_4 polyhedron. The $P2_1/c$ structure (Figure 1 c)) is characterized by $\text{Sn}_4\text{Ch}_4\text{X}_8$ units which are composed of four pyramids: SnChX_4 - SnCh_3X_2 - SnCh_3X_2 - SnChX_4 . SnChX_4 and SnCh_3X_2 share faces and the two SnCh_3X_2 units edges. Along the c axis, two neighbouring $\text{Sn}_4\text{Ch}_4\text{X}_8$ units are linked by two M(III) atoms, each forming a square pyramidal $\text{M(III)Ch}_3\text{X}_2$. In addition, neighbouring $\text{Sn}_4\text{Ch}_4\text{X}_8$ units share corners (X) along the b direction, thus forming a 2D $\text{Sn}_4\text{M(III)}_2\text{Ch}_4\text{X}_6$ structure within the bc plane.

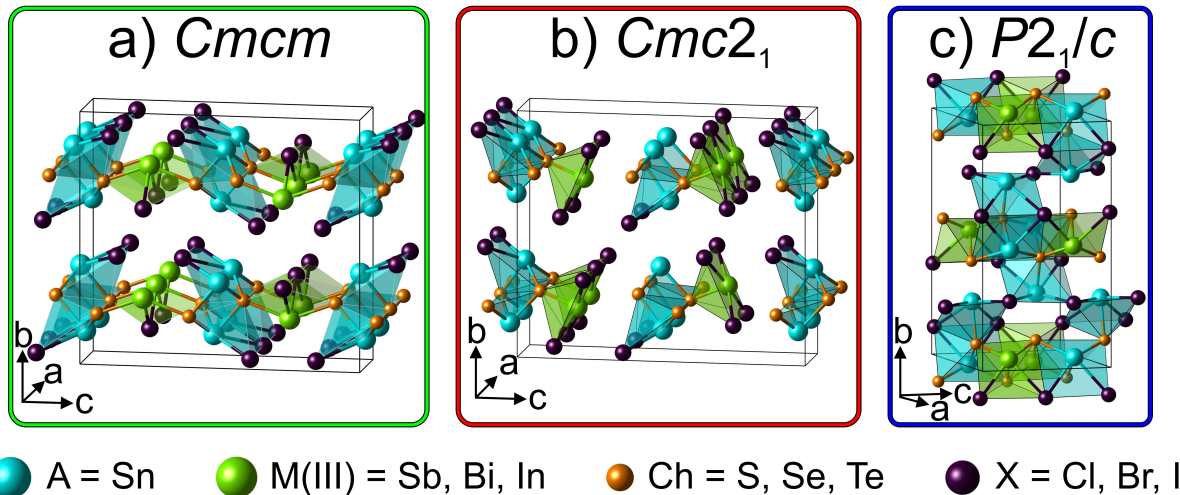


Figure 1: Visualization of the $\text{Sn}_2\text{M(III)Ch}_2\text{X}_3$ structure in different space groups; a) $Cmcm$, b) $Cmc2_1$ and c) $P2_1/c$ for the example of $\text{Sn}_2\text{SbS}_2\text{I}_3$. The coordinating polyhedrons associated with the Sn/(A) positions are depicted in cyan and those associated with the M(III) position in green. The coordinates of each space group were taken from the Materials Project⁵⁶ and were visualized with VESTA.⁵⁷

We generated the initial structures of the individual $\text{Sn}_2\text{M(III)Ch}_2\text{X}_3$ compounds from those of known materials listed in the Materials Project.⁵⁶ For $Cmcm$ and $Cmc2_1$, we adopted the $\text{Sn}_2\text{SbS}_2\text{I}_3$ structures (ref. numbers: mp-561134 and mp-1219046) and for $P2_1/c$, the $\text{Pb}_2\text{SbS}_2\text{I}_3$ structure (ref. number: mp-578882). We then replaced any Pb by Sn and carried out corresponding replacements on the M(III), Ch and X positions to generate a total of 27 $\text{Sn}_2\text{M(III)Ch}_2\text{X}_3$ compounds per space group. These were then geometry-optimized with PBEsol before we computed the electronic structure with HSE06+SOC.

2.3 Screening criteria

The aim of this study is to screen the mixed-metal chalcogenides $\text{Sn}_2\text{M(III)Ch}_2\text{X}_3$ material space for compounds that are suitable for photovoltaic applications and have the potential to increase their PCE. We first consider formation energies to estimate the materials' chemical stability. Chemical stability itself is hard to quantify, because it depends on the temperature, the chemical space, the synthesis process and the environmental conditions. To first order, we therefore approximate the chemical stability by the thermodynamic stability with respect to elementary decomposition computed at 0 K as expressed in Eq. (1). This allows us to draw first conclusions about the energetic preference of $\text{Sn}_2\text{M(III)Ch}_2\text{X}_3$ compounds.

The band gap should be in the range of 1.0–1.8 eV for outdoor or 1.5–2.0 eV for indoor photovoltaics^{24,58} according to the Shockley-Queisser limit. In our DFT calculations, we observe a difference of around 0.3 eV between the fundamental and the optical band gap for some $\text{Sn}_2\text{M(III)Ch}_2\text{X}_3$ materials (see discussion in Sec. 3.1). We therefore set a target range of 0.7–2.0 eV to encompass indoor and outdoor photovoltaic applications and incorporate the ~ 0.3 eV shift.

2.4 Novelty check

To ascertain which materials in the $\text{Sn}_2\text{M(III)Ch}_2\text{X}_3$ space have already been made or are known, we query a variety of materials databases. The OPTIMADE python API^{59,60} provides an easy way to search a selection of databases with a single query. Our search includes the following 16 databases: Automatic FLOW for Materials Discovery (AFLOW),^{61,62} Alexandria, Computational materials repository (CMR), Crystallography Open Database (COD),^{63,64} Cambridge Crystallographic Database (CCD),⁶⁵ Inorganic Crystal Structure Database (ICSD),^{66–69} Joint Automated Repository for Various Integrated Simulations (JARVIS),⁷⁰ Materials Cloud,^{71–73} Materials Project,⁵⁶ Materials Platform for Data Science (MPDS), Novel Materials Discovery Laboratory (NOMAD),^{74,75} Open Database of Xtals (odbx),⁷⁶ Open Materials Database (omdb),⁷⁷ Open Quantum Materials Database

(OQMD)⁷⁸ Theoretical Crystallography Open Database (TCOD),⁷⁹ and 2D Materials Encyclopedia.⁸⁰ In addition, we also included in our search the DCGAT-3 dataset by Schmidt *et al.*, which was used to train their 3rd generation crystal-graph attention network and includes about 3.18 million crystalline compounds, including a large number of quaternary materials.³¹

3 Results and discussion

3.1 Promising Sn₂M(III)Ch₂X₃ materials

Sn₂SbS₂I₃ has already been studied with DFT by Kavanagh *et al.*¹¹ and Nicolson *et al.*¹⁷, which provides us with an opportunity to validate our computational approach. Our PBEsol results for the energy differences between the *Cmc2₁* and *P2₁/c* phases and the *Cmcm* phase are reported in Table 1 and are in good agreement with the optB86b-vdW results of Kavanagh and Nicolson.

Table 1: Relative energies of both *Cmc2₁* and *P2₁/c* phases of Sn₂SbS₂I₃ with respect to the *Cmcm* phase (given in meV atom⁻¹). The energy of the reference *Cmcm* phase is set to 0. Previous DFT results are included for comparison. Fundamental band gaps for *Cmcm*, *Cmc2₁* and *P2₁/c* (given in eV). Indirect band gaps are marked with an *.

	ΔE_{form} (<i>Cmc2₁</i>)	ΔE_{form} (<i>P2₁/c</i>)	Functional	E_g (<i>Cmcm</i>)	E_g (<i>Cmc2₁</i>)	E_g (<i>P2₁/c</i>)	Functional
Kavanagh <i>et al.</i> ¹¹	-36	-/-	optB86b-vdW	1.02*	1.08	-/-	HSE06+SOC
Nicolson <i>et al.</i> ¹⁷	-11	-71	optB86b-vdW	-/-	-/-	1.78*	HSE06+SOC
Our work	-11	-69	PBEsol	0.947*	1.007	1.686*	HSE06+SOC

Our band gap values calculated with HSE06 for Sn₂SbS₂I₃ agree well with literature for all three phases, see Table 1. A direct gap is determined for *Cmc2₁* and indirect gaps for *Cmcm* and *P2₁/c*.

In addition, Kavanagh *et al.* reported that the absorption edge is larger than the fundamental band gap for Sn₂SbS₂I₃. The authors proposed two reasons: I) a low density of states at the band edges caused by a low electronic degeneracy due to the low crystal symmetry (for *Cmcm* and *Cmc2₁*) and II) a weak transition dipole moment between the valence

band maximum and the conduction band minimum due to the symmetry restrictions and a low spatial overlap.¹¹ As a result, the absorption intensity is very low at the onset of absorption close to the fundamental band gap. It then rises slowly as the joint density of states increases. Appreciable absorption intensity is then only observed at some tenth of eV above the fundamental gap. To check if this behavior translates to other compounds in the $\text{Sn}_2\text{M(III)Ch}_2\text{X}_3$ family, we calculated the absorption spectra for all 27 candidates. As an example, the absorption spectrum and the corresponding Tauc plot for $\text{Sn}_2\text{InS}_2\text{Br}_3$ in the $Cmcm$ phase is shown in Figure 2. The intensity at the fundamental band gap is weak but not zero. It then increases rapidly at $E_g + \sim 0.4$, which is most evident in panel b). We define this transition point as “optical gap”. From the Tauc plot, we deduce that the optical gap lies 0.36 eV above the fundamental gap for $\text{Sn}_2\text{InS}_2\text{Br}_3$. The corresponding band structure is shown in Figure 1 of the SI.

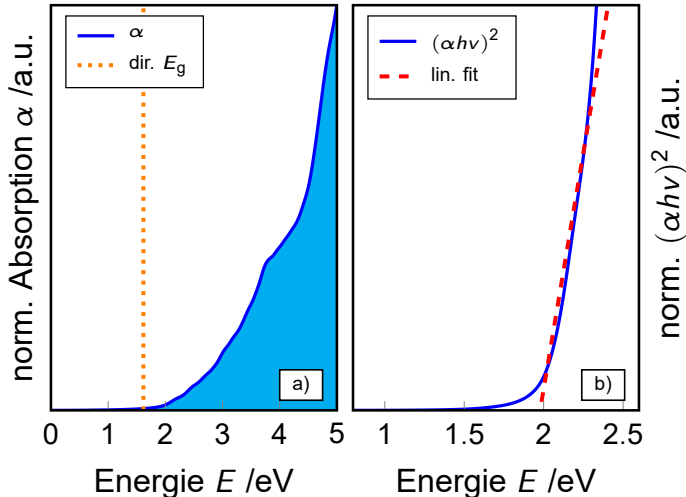


Figure 2: Absorption spectrum normalized to 5 eV (a) and resulting Tauc plot (b) (HSE06+SOC level of theory) for $\text{Sn}_2\text{InS}_2\text{Br}_3$ within the $Cmcm$ phase. The orange line in a) indicates the calculated fundamental band gap of 1.617 eV and the red line in b) the best linear fit ($R^2 = 0.955$) resulting in an optical band gap of ~ 1.977 eV.

For all 27 $\text{Sn}_2\text{M(III)Ch}_2\text{X}_3$ materials we find a larger optical gap, see Table 1 in the SI. For compounds with a direct band gap, the optical band gap lies on average 0.291 eV above the fundamental gap. This difference is space group dependent with ~ 0.376 eV for $Cmcm$ and $Cmc2_1$ and ~ 0.123 eV for $P2_1/c$. For indirect band gap materials, the optical gap

is also larger than the indirect fundamental gap ($E_{g, \text{ind}}$). However, if we compare to the lowest direct gap ($E_{g, \text{dir}}$), the difference to the optical gap is only 0.049 eV on average and nearly identical for all space groups. This is caused by an increased spatial overlap between the valence band maximum and the conduction band. Therefore, our band gap criterion considers not only the slightly different ranges for indoor and outdoor photovoltaics, but also the difference between the fundamental band gap and the absorption edge (see Section 2.3).

Our DFT calculations of the $\text{Sn}_2\text{M(III)Ch}_2\text{X}_3$ materials space subsequently identified 12 compounds that satisfy the screening criteria of thermodynamic stability (negative formation energy at 0 K) and fundamental direct band gap (in the range of 0.7–2.0 eV): $\text{Sn}_2\text{InS}_2\text{Br}_3$, $\text{Sn}_2\text{InS}_2\text{I}_3$, $\text{Sn}_2\text{InSe}_2\text{Cl}_3$, $\text{Sn}_2\text{InSe}_2\text{Br}_3$, $\text{Sn}_2\text{InTe}_2\text{Br}_3$, $\text{Sn}_2\text{InTe}_2\text{Cl}_3$, $\text{Sn}_2\text{SbS}_2\text{I}_3$, $\text{Sn}_2\text{SbSe}_2\text{Cl}_3$, $\text{Sn}_2\text{SbSe}_2\text{I}_3$, $\text{Sn}_2\text{SbTe}_2\text{Cl}_3$, $\text{Sn}_2\text{BiS}_2\text{I}_3$ and $\text{Sn}_2\text{BiTe}_2\text{Cl}_3$. The formation energies of the 12 compounds in all three considered space groups are illustrated in Figure 3. A detailed overview of the formation energies of all 27 $\text{Sn}_2\text{M(III)Ch}_2\text{X}_3$ compounds, as well as their lattice parameters, fundamental band and optical band gaps, is reported in Table 1 of the SI.

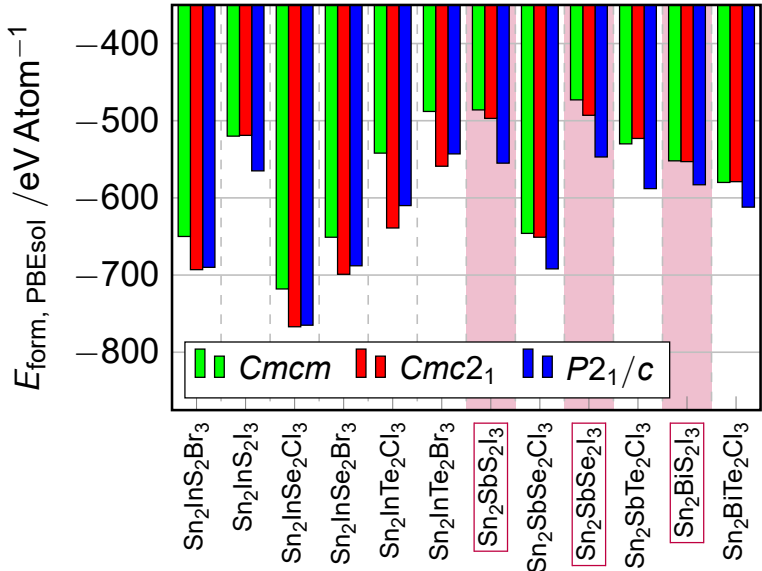


Figure 3: Formation energy (calculated with PBEsol) of the 12 $\text{Sn}_2\text{M(III)Ch}_2\text{X}_3$ materials of interest for $Cmc1$ (green), $Cmc2_1$ (red) and $P2_1/c$ (blue) space groups. Three structures - $\text{Sn}_2\text{SbS}_2\text{I}_3$,¹⁶ $\text{Sn}_2\text{SbSe}_2\text{I}_3$,¹⁸ and $\text{Sn}_2\text{BiS}_2\text{I}_3$ ¹⁹ - that are already known from the literature, are highlighted in purple.

All of the 27 $\text{Sn}_2\text{M(III)Ch}_2\text{X}_3$ structures are stable with respect to elemental decomposition (see Table 1 of the SI) but not all fall into the desired band gap range. For the 12 candidates the most stable material is $\text{Sn}_2\text{InSe}_2\text{Cl}_3$ (-718 , -767 , and -765 meV atom $^{-1}$ for $Cmcm$, $Cmc2_1$, and $P2_1/c$, respectively). The In-based compounds are in most cases significantly more stable than their Sb- and Bi-based counterparts with the $Cmc2_1$ phase being preferred. $\text{Sn}_2\text{InS}_2\text{I}_3$, in which the $P2_1/c$ structure is most stable, is an exception. For the Sb or Bi compounds, the $P2_1/c$ phase is the most stable. The formation energy decreases from $\text{Sn}_2\text{M(III)Ch}_2\text{Cl}_3$ over $\text{Sn}_2\text{M(III)Ch}_2\text{Br}_3$ towards $\text{Sn}_2\text{M(III)Ch}_2\text{I}_3$, which is natural as Cl forms the strongest metal-halide bonds due to the highest electronegativity among the three halogen elements.

An analogous behavior is obtained for 15 $\text{Sn}_2\text{M(III)Ch}_2\text{X}_3$ compounds with an indirect fundamental gap (which we refer to as indirect $\text{Sn}_2\text{M(III)Ch}_2\text{X}_3$): $\text{Sn}_2\text{InS}_2\text{Cl}_3$, $\text{Sn}_2\text{InSe}_2\text{I}_3$, $\text{Sn}_2\text{InTe}_2\text{I}_3$, $\text{Sn}_2\text{SbS}_2\text{Cl}_3$, $\text{Sn}_2\text{SbS}_2\text{Br}_3$, $\text{Sn}_2\text{SbSe}_2\text{Br}_3$, $\text{Sn}_2\text{SbTe}_2\text{Br}_3$, $\text{Sn}_2\text{SbTe}_2\text{I}_3$, $\text{Sn}_2\text{BiS}_2\text{Cl}_3$, $\text{Sn}_2\text{BiS}_2\text{Br}_3$, $\text{Sn}_2\text{BiSe}_2\text{Cl}_3$, $\text{Sn}_2\text{BiSe}_2\text{Br}_3$, $\text{Sn}_2\text{BiSe}_2\text{I}_3$, $\text{Sn}_2\text{BiTe}_2\text{Br}_3$ and $\text{Sn}_2\text{BiTe}_2\text{I}_3$. The lowest direct gap in these 15 materials is also within the screening range of 0.7–2.0 eV. Their formation energies are reported in Figure 2 and Table 1 in the SI.

Our band gap results of the 27 $\text{Sn}_2\text{M(III)Ch}_2\text{X}_3$ materials reveal that the space group influences the nature of the gap. For example, for $\text{Sn}_2\text{InS}_2\text{Br}_3$ the $Cmcm$ and $Cmc2_1$ structures have a direct band gap, but not $P2_1/c$. However, replacing S with Se leads to a direct band gap for the $Cmcm$ structure and an indirect band gap for the other two structures. Overall, it turns out that all 12 identified materials have at least one space group with an indirect band gap. In Figure 4 the direct band gaps for the 12 $\text{Sn}_2\text{M(III)Ch}_2\text{X}_3$ materials are shown.

The $Cmcm$ and $Cmc2_1$ phases tend to have direct band gaps, whereas $P2_1/c$ structures exhibit indirect gaps. As a result, only two $P2_1/c$ compounds ($\text{Sn}_2\text{InTe}_2\text{Cl}_3$ and $\text{Sn}_2\text{InTe}_2\text{Br}_3$) fall into our targeted band gap region. Also the band gap values depend on the space-group. Gaps of $Cmc2_1$ structures lie around 1 eV except for $\text{Sn}_2\text{InS}_2\text{Br}_3$. In contrast, $Cmcm$ phases

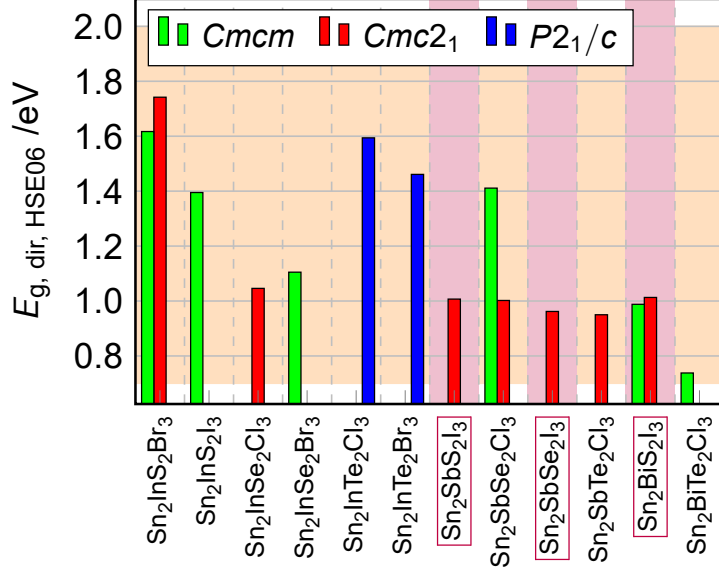


Figure 4: Direct band gaps (HSE06+SOC level of theory) for 11 Sn₂SbS₂I₃ materials of interest for *Cmcm* (green), *Cmc2₁* (red) and *P2₁/c* (blue) space groups. Three structures - Sn₂SbS₂I₃,¹⁶ Sn₂SbSe₂I₃,¹⁸ and Sn₂BiS₂I₃¹⁹ - that are already known from the literature, are highlighted in purple.

have larger band gaps $\sim 1.4\text{--}1.5\text{ eV}$ with the exception of Sn₂BiS₂I₃ and Sn₂InSe₂Br₃. In general, direct band gaps are largest for *P2₁/c* and smallest for *Cmc2₁* with *Cmcm* in between (see also Table 2). A similar picture emerges for the lowest direct band gaps in indirect gap materials (see Table 2 and Figure 3 of the SI).

In sum, our results indicate that the band gaps of indium-based Sn₂M(III)Ch₂X₃ compounds lie in the middle and upper region of our screening range, making them interesting for both indoor and outdoor photovoltaics. However, the scarcity of indium becomes a cost factor, whereby a number of efforts are underway to ensure the long-term supply of indium through significant changes in processing and recycling. With band gaps around 1 eV antimony and bismuth-based Sn₂M(III)Ch₂X₃ materials would be interesting for outdoor photovoltaics. Considering antimony's toxicity, bismuth-based Sn₂M(III)Ch₂X₃ materials might be promising contenders.

Lastly, we check which Sn₂M(III)Ch₂X₃ materials are already known or have appeared in databases or datasets. Our search reveals that only three materials have been reported

Table 2: Fundamental and optical band gaps ($E_{g, \text{opt}}$) [given in eV] of $\text{Sn}_2\text{M(III)Ch}_2\text{X}_3$ which have been identified as interesting. For indirect compounds the band gap of the lowest direct transition ($E_{g, \text{dir}}$) as well as of the lowest indirect transition ($E_{g, \text{ind}}$) are provided. $\text{Sn}_2\text{M(III)Ch}_2\text{X}_3$ materials with a direct fundamental band gap are colored in orange and these with an indirect one in gray.

		$\text{Sn}_2\text{InS}_2\text{Cl}_3$	$\text{Sn}_2\text{InS}_2\text{Br}_3$	$\text{Sn}_2\text{InS}_2\text{I}_3$	$\text{Sn}_2\text{InSe}_2\text{Cl}_3$	$\text{Sn}_2\text{InSe}_2\text{Br}_3$	$\text{Sn}_2\text{InSe}_2\text{I}_3$	$\text{Sn}_2\text{InTe}_2\text{Cl}_3$	$\text{Sn}_2\text{InTe}_2\text{Br}_3$	$\text{Sn}_2\text{InTe}_2\text{I}_3$	$\text{Sn}_2\text{SbS}_2\text{Cl}_3$	$\text{Sn}_2\text{SbS}_2\text{Br}_3$	$\text{Sn}_2\text{SbS}_2\text{I}_3$	$\text{Sn}_2\text{SbSe}_2\text{Cl}_3$	$\text{Sn}_2\text{SbSe}_2\text{Br}_3$
<i>Cmcm</i>	$E_{g, \text{dir}}$	1.305	1.617	1.395	-/-	1.105	1.369	-/-	-/-	1.089	1.679	1.474	0.997	1.411	1.412
	$E_{g, \text{ind}}$	1.251	-/-	-/-	-/-	-/-	1.299	-/-	-/-	0.994	1.611	0.883	0.947	-/-	1.330
	$E_{g, \text{opt}}$	1.491	1.977	1.934	-/-	1.477	1.397	-/-	-/-	1.126	1.773	1.527	1.547	1.816	1.504
<i>Cmc2₁</i>	$E_{g, \text{dir}}$	1.834	1.742	1.12	1.046	1.373	-/-	0.915	-/-	0.867	1.242	1.248	1.007	1.002	0.941
	$E_{g, \text{ind}}$	1.692	-/-	0.598	-/-	1.338	-/-	0.804	-/-	0.802	1.056	1.055	-/-	-/-	0.891
	$E_{g, \text{opt}}$	1.887	1.783	1.187	1.684	1.396	-/-	1.011	-/-	0.964	1.288	1.344	1.506	1.261	1.044
<i>P2₁/c</i>	$E_{g, \text{dir}}$	-/-	1.985	-/-	-/-	1.843	1.947	1.594	1.461	1.109	-/-	-/-	1.762	-/-	2.028
	$E_{g, \text{ind}}$	-/-	1.616	-/-	-/-	1.488	1.785	-/-	-/-	1.083	-/-	-/-	1.686	-/-	1.642
	$E_{g, \text{opt}}$	-/-	1.996	-/-	-/-	1.855	1.960	1.713	1.592	1.201	-/-	-/-	1.771	-/-	2.100

		$\text{Sn}_2\text{SbSe}_2\text{I}_3$	$\text{Sn}_2\text{SbTe}_2\text{Cl}_3$	$\text{Sn}_2\text{SbTe}_2\text{Br}_3$	$\text{Sn}_2\text{SbTe}_2\text{I}_3$	$\text{Sn}_2\text{BiS}_2\text{Cl}_3$	$\text{Sn}_2\text{BiS}_2\text{Br}_3$	$\text{Sn}_2\text{BiS}_2\text{I}_3$	$\text{Sn}_2\text{BiSe}_2\text{Cl}_3$	$\text{Sn}_2\text{BiSe}_2\text{Br}_3$	$\text{Sn}_2\text{BiSe}_2\text{I}_3$	$\text{Sn}_2\text{BiTe}_2\text{Cl}_3$	$\text{Sn}_2\text{BiTe}_2\text{Br}_3$	$\text{Sn}_2\text{BiTe}_2\text{I}_3$
<i>Cmcm</i>	$E_{g, \text{dir}}$	1.057	0.943	-/-	0.786	1.535	1.343	0.988	1.104	0.965	1.048	0.738	0.852	-/-
	$E_{g, \text{ind}}$	0.800	1.874	-/-	0.465	0.986	0.956	-/-	1.096	0.666	0.769	-/-	0.715	-/-
	$E_{g, \text{opt}}$	1.056	1.997	-/-	0.795	1.548	1.434	1.390	1.124	1.063	1.141	1.059	0.854	-/-
<i>Cmc2₁</i>	$E_{g, \text{dir}}$	0.962	0.950	1.027	-/-	1.146	1.405	1.013	0.902	1.841	1.064	0.852	0.854	-/-
	$E_{g, \text{ind}}$	-/-	-/-	0.980	-/-	1.034	1.124	-/-	0.714	0.827	0.881	0.715	0.718	-/-
	$E_{g, \text{opt}}$	1.640	1.370	1.063	-/-	1.169	1.504	1.420	0.952	0.853	1.162	0.854	0.856	-/-
<i>P2₁/c</i>	$E_{g, \text{dir}}$	1.892	-/-	-/-	-/-	-/-	1.968	1.606	1.196	1.425	1.660	-/-	-/-	0.890
	$E_{g, \text{ind}}$	1.672	-/-	-/-	-/-	-/-	1.717	1.490	1.076	1.118	1.474	-/-	-/-	0.256
	$E_{g, \text{opt}}$	1.983	-/-	-/-	-/-	-/-	2.065	1.599	1.254	1.452	1.751	-/-	-/-	0.931

so far: $\text{Sn}_2\text{SbS}_2\text{I}_3$,¹⁶ $\text{Sn}_2\text{SbSe}_2\text{I}_3$ ¹⁸ and $\text{Sn}_2\text{BiS}_2\text{I}_3$.¹⁹ For $\text{Sn}_2\text{SbS}_2\text{I}_3$, structures in all three space groups are known, but for the other two only *Cmcm* and *Cmc2₁* have been reported. To the best of our knowledge we are the first to present the eight direct band gaps materials ($\text{Sn}_2\text{InS}_2\text{Br}_3$, $\text{Sn}_2\text{InS}_2\text{I}_3$, $\text{Sn}_2\text{InSe}_2\text{Cl}_3$, $\text{Sn}_2\text{InSe}_2\text{Br}_3$, $\text{Sn}_2\text{InTe}_2\text{Br}_3$, $\text{Sn}_2\text{InTe}_2\text{Cl}_3$, $\text{Sn}_2\text{SbSe}_2\text{Cl}_3$ and $\text{Sn}_2\text{SbTe}_2\text{Cl}_3$) and the 12 $\text{Sn}_2\text{M(III)Ch}_2\text{X}_3$ indirect band gaps materials ($\text{Sn}_2\text{InS}_2\text{Cl}_3$, $\text{Sn}_2\text{InSe}_2\text{I}_3$, $\text{Sn}_2\text{InTe}_2\text{I}_3$, $\text{Sn}_2\text{SbS}_2\text{Cl}_3$, $\text{Sn}_2\text{SbS}_2\text{Br}_3$, $\text{Sn}_2\text{SbSe}_2\text{Br}_3$, $\text{Sn}_2\text{SbTe}_2\text{Br}_3$, $\text{Sn}_2\text{BiS}_2\text{Cl}_3$, $\text{Sn}_2\text{BiS}_2\text{Br}_3$, $\text{Sn}_2\text{BiSe}_2\text{Cl}_3$, $\text{Sn}_2\text{BiSe}_2\text{Br}_3$ and $\text{Sn}_2\text{BiSe}_2\text{I}_3$).

3.2 Promising $\text{Sn}_2\text{M(III)}_{1-a}\text{M(III)}'_a\text{Ch}_{2-b}\text{Ch}'_b\text{X}_{3-c}\text{X}'_c$ alloys

In this section we extend the materials space to possible binary $\text{Sn}_2\text{M(III)}_{1-a}\text{M(III)}'_a\text{Ch}_{2-b}\text{Ch}'_b\text{X}_{3-c}\text{X}'_c$ alloys with band gaps in the desired range. We

consider alloys within the same space group for which I) at least one compound has a direct band gap in the target range or II) one compound has a direct band gap below 0.7 eV and the another above 2 eV. We identified 12 $\text{Sn}_2\text{M}(\text{III})_{1-a}\text{M}(\text{III})'_a\text{Ch}_{2-b}\text{Ch}'_b\text{X}_{3-c}\text{X}'_c$ suitable alloys (see Figure 5). We expect direct band gaps in at least a part of the compositions. With such alloys, the band gap could be tuned for specific optoelectronic applications. To the best of our knowledge, none of these binary $\text{Sn}_2\text{M}(\text{III})_{1-a}\text{M}(\text{III})'_a\text{Ch}_{2-b}\text{Ch}'_b\text{X}_{3-c}\text{X}'_c$ alloy compounds have been studied in the literature yet.

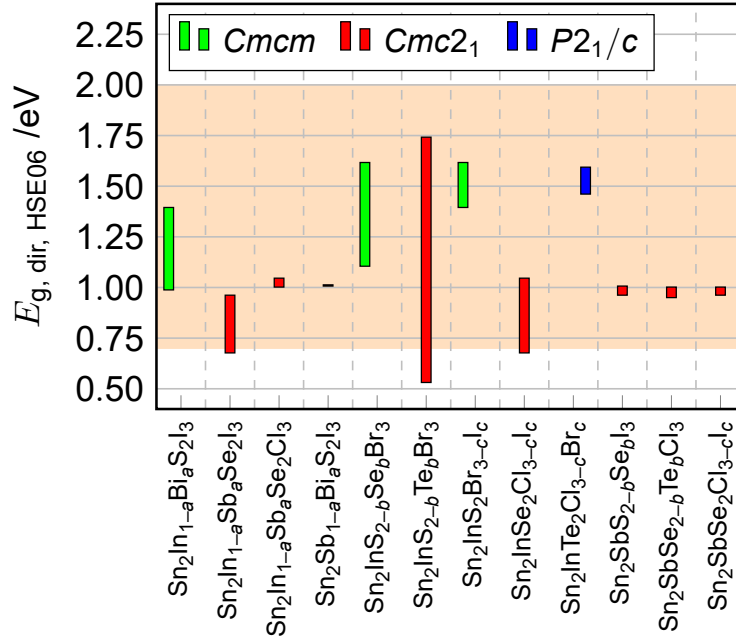


Figure 5: Band gap ranges (HSE06+SOC level of theory) for the 12 $\text{Sn}_2\text{M}(\text{III})_{1-a}\text{M}(\text{III})'_a\text{Ch}_{2-b}\text{Ch}'_b\text{X}_{3-c}\text{X}'_c$ binary alloys of interest for $Cmcm$ (green), $Cmc2_1$ (red) and $P2_1/c$ (blue) space groups.

We find that the $Cmc2_1$ space group is most prevalent followed by $Cmcm$. Only a single binary alloy has the $P2_1/c$ space group because of the phase's preference for indirect gaps. Materials in the $Cmc2_1$ space group tend towards lower band gaps close to ~ 1 eV, because the parent compounds have small gaps. One exception is $\text{Sn}_2\text{InS}_{2-b}\text{Te}_b\text{Br}_3$ which combines $\text{Sn}_2\text{InTe}_2\text{Br}_3$ ($E_g = 0.531$ eV) and $\text{Sn}_2\text{InTe}_2\text{Br}_3$ ($E_g = 1.742$ eV), resulting in a broad range of 1.211 eV. For the three $Cmcm$ alloys, we find $\text{Sn}_2\text{In}_{1-a}\text{Bi}_a\text{S}_2\text{I}_3$ at the lower end, $\text{Sn}_2\text{InS}_{2-b}\text{Se}_b\text{Br}_3$ and $\text{Sn}_2\text{InS}_2\text{Br}_{3-clc}$ in the middle of the range. If we

drop our restriction of mixing compounds with a direct gap, we obtain an additional 69 $\text{Sn}_2\text{M}(\text{III})_{1-a}\text{M}(\text{III})'_a\text{Ch}_{2-b}\text{Ch}'_b\text{X}_{3-c}\text{X}'_c$ alloys reported in Figure 4 of the SI.

Our results indicate that $\text{Sn}_2\text{M}(\text{III})_{1-a}\text{M}(\text{III})'_a\text{Ch}_{2-b}\text{Ch}'_b\text{X}_{3-c}\text{X}'_c$ alloys with indium and iodine offer the most flexibility (i.e. widest tuning ranges). However, considering the scarcity of indium and the relatively high toxicity of antimony, alloys with bismuth would be favoured. Since we could not identify a suitable bismuth alloy, $\text{Sn}_2\text{In}_{1-a}\text{Bi}_a\text{S}_2\text{I}_3$ might offer the best, environmentally friendly compromise.

4 Conclusion

In the pursuit of low-toxicity photovoltaic materials, we used DFT to explore the $\text{Sn}_2\text{M}(\text{III})\text{Ch}_2\text{X}_3$ material space. We identified 12 absorbers that fulfill our requirements by being a lead-free, thermodynamically stable and with a direct band gap in the screening range of 0.7–2.0 eV. Three of these $\text{Sn}_2\text{M}(\text{III})\text{Ch}_2\text{X}_3$ were known previously, while the remaining nine materials, i.e., $\text{Sn}_2\text{InS}_2\text{Br}_3$, $\text{Sn}_2\text{InS}_2\text{I}_3$, $\text{Sn}_2\text{InSe}_2\text{Cl}_3$, $\text{Sn}_2\text{InSe}_2\text{Br}_3$, $\text{Sn}_2\text{InTe}_2\text{Br}_3$, $\text{Sn}_2\text{InTe}_2\text{Cl}_3$, $\text{Sn}_2\text{SbSe}_2\text{Cl}_3$, $\text{Sn}_2\text{SbTe}_2\text{Cl}_3$ and $\text{Sn}_2\text{BiTe}_2\text{Cl}_3$, are reported here for the first time. The majority of these compounds contain indium, including some of the most promising candidates, like $\text{Sn}_2\text{InSe}_2\text{Br}_3$ or $\text{Sn}_2\text{InS}_2\text{Br}_3$. An alternative to indium- and antimony-based $\text{Sn}_2\text{M}(\text{III})\text{Ch}_2\text{X}_3$ materials are bismuth-based ones, such as e.g., $\text{Sn}_2\text{BiTe}_2\text{Cl}_3$, although the band gap is smaller than its indium-based counterparts. In addition, we identified 15 previously unknown $\text{Sn}_2\text{M}(\text{III})\text{Ch}_2\text{X}_3$ compounds with indirect band gaps, which have a lowest direct band gap within the screening range.

We investigated the potential to tune the band gap by exploring $\text{Sn}_2\text{M}(\text{III})_{1-a}\text{M}(\text{III})'_a\text{Ch}_{2-b}\text{Ch}'_b\text{X}_{3-c}\text{X}'_c$ alloys. In total, 12 $\text{Sn}_2\text{M}(\text{III})_{1-a}\text{M}(\text{III})'_a\text{Ch}_{2-b}\text{Ch}'_b\text{X}_{3-c}\text{X}'_c$ alloys were identified by alloying within the same phase and considering only structures with direct gaps. For example, the fundamental gap of $\text{SnIn}_{1-a}\text{Bi}_a\text{S}_2\text{Br}_3$ can be tuned between 0.988–1.395 eV. Furthermore, we identified

additional 69 $\text{Sn}_2\text{M}(\text{III})_{1-a}\text{M}(\text{III})'_a\text{Ch}_{2-b}\text{Ch}'_b\text{X}_{3-c}\text{X}'_c$ alloys by dropping our requirement to use only direct band gap $\text{Sn}_2\text{M}(\text{III})\text{Ch}_2\text{X}_3$ end structures, which broadens significantly the $\text{Sn}_2\text{M}(\text{III})_{1-a}\text{M}(\text{III})'_a\text{Ch}_{2-b}\text{Ch}'_b\text{X}_{3-c}\text{X}'_c$ spectra.

Our findings highlight the relevance of materials design and theoretical explorations, and the identified $\text{Sn}_2\text{M}(\text{III})\text{Ch}_2\text{X}_3$ materials and $\text{Sn}_2\text{M}(\text{III})_{1-a}\text{M}(\text{III})'_a\text{Ch}_{2-b}\text{Ch}'_b\text{X}_{3-c}\text{X}'_c$ alloys encourage the synthesis and the use of highly stable materials in various optoelectronic devices.

Acknowledgement

The authors thank Milica Todorović and Armi Tiihonen for fruitful discussions. This study was supported by the Academy of Finland through Project No. 334532 and the National Natural Science Foundation of China (Grant No. 62281330043). PH, JL and PR further acknowledge CSC-IT Center for Science, Finland, the Aalto Science-IT project, Xi'an Jiaotong University's HPC platform and the Hefei Advanced Computing Center of China for generous computational resources. PV acknowledges the financial support of Academy of Finland, Decision No. 347772. This work is part of the Academy of Finland Flagship Programme, Photonics Research and Innovation (PREIN), Decision No. 320165. GKG acknowledges Tampere Institute for Advanced Study for postdoctoral funding.

Supporting Information Available

The Supporting Information is available free of charge at ...

- band structure for $\text{Sn}_2\text{InS}_2\text{Br}_3$ ($Cmcm$)
- lattice parameters, formation energies, fundamental (direct and indirect) and optical gaps for all $\text{Sn}_2\text{M(III)Ch}_2\text{X}_3$ materials
- formation energies of indirect $\text{Sn}_2\text{M(III)Ch}_2\text{X}_3$ materials
- band gaps for all $\text{Sn}_2\text{M(III)Ch}_2\text{X}_3$ materials and $\text{Sn}_2\text{M(III)}_{1-a}\text{M(III)}'_a\text{Ch}_{2-b}\text{Ch}'_b\text{X}_{3-c}\text{X}'_c$ alloys

Notes

The authors declare no competing financial interest.

References

- (1) Huang, Y.-T.; Kavanagh, S. R.; Scanlon, D. O.; Walsh, A.; Hoye, R. L. Z. Perovskite-Inspired Materials for Photovoltaics and beyond—from Design to Devices. *Nanotechnology* **2021**, *32*, 132004.
- (2) Huang, Y.-T.; Kavanagh, S. R.; Scanlon, D. O.; Walsh, A.; Hoye, R. L. Z. Corrigendum: Perovskite-inspired Materials for Photovoltaics and beyond—from Design to Devices (2021 Nanotechnology 32 132004). *Nanotechnology* **2021**, *32*, 379501.
- (3) Ganose, A. M.; Savory, C. N.; Scanlon, D. O. Beyond Methylammonium Lead Iodide: Prospects for the Emergent Field of Ns^2 Containing Solar Absorbers. *Chemical Communications* **2017**, *53*, 20–44.
- (4) Nie, R.; Sumukam, R. R.; Reddy, S. H.; Banavoth, M.; Seok, S. I. Lead-Free Perovskite Solar Cells Enabled by Hetero-Valent Substitutes. *Energy & Environmental Science* **2020**, *13*, 2363–2385.
- (5) Cao, J.; Yan, F. Recent Progress in Tin-Based Perovskite Solar Cells. *Energy & Environmental Science* **2021**, *14*, 1286–1325.
- (6) Brandt, R. E.; Poindexter, J. R.; Gorai, P.; Kurchin, R. C.; Hoye, R. L. Z.; Nienhaus, L.; Wilson, M. W. B.; Polizzotti, J. A.; Sereika, R.; Žaltauskas, R.; Lee, L. C.; MacManus-Driscoll, J. L.; Bawendi, M.; Stevanović, V.; Buonassisi, T. Searching for “Defect-Tolerant” Photovoltaic Materials: Combined Theoretical and Experimental Screening. *Chemistry of Materials* **2017**, *29*, 4667–4674.
- (7) Rondiya, S. R.; Jagt, R. A.; MacManus-Driscoll, J. L.; Walsh, A.; Hoye, R. L. Z. Self-Trapping in Bismuth-Based Semiconductors: Opportunities and Challenges from Optoelectronic Devices to Quantum Technologies. *Applied Physics Letters* **2021**, *119*, 220501.

- (8) Im, S. H.; Kim, H.-j.; Kim, S. W.; Kim, S.-W.; Seok, S. I. All Solid State Multiply Layered PbS Colloidal Quantum-Dot-Sensitized Photovoltaic Cells. *Energy & Environmental Science* **2011**, *4*, 4181.
- (9) Lee, Y.-L.; Lo, Y.-S. Highly Efficient Quantum-Dot-Sensitized Solar Cell Based on Co-Sensitization of CdS/CdSe. *Advanced Functional Materials* **2009**, *19*, 604–609.
- (10) Choi, Y. C.; Lee, D. U.; Noh, J. H.; Kim, E. K.; Seok, S. I. Highly Improved Sb₂S₃ Sensitized-Inorganic-Organic Heterojunction Solar Cells and Quantification of Traps by Deep-Level Transient Spectroscopy. *Advanced Functional Materials* **2014**, *24*, 3587–3592.
- (11) Kavanagh, S. R.; Savory, C. N.; Scanlon, D. O.; Walsh, A. Hidden Spontaneous Polarisation in the Chalcogenide Photovoltaic Absorber Sn₂SbS₂I₃. *Materials Horizons* **2021**, *8*, 2709–2716.
- (12) Nie, R.; Lee, K. S.; Hu, M.; Paik, M. J.; Seok, S. I. Heteroleptic Tin-Antimony Sulfoiodide for Stable and Lead-free Solar Cells. *Matter* **2020**, *3*, 1701–1713.
- (13) Sopiha, K. V.; Comparotto, C.; Márquez, J. A.; Scragg, J. J. S. Chalcogenide Perovskites: Tantalizing Prospects, Challenging Materials. *Advanced Optical Materials* **2022**, *10*, 2101704.
- (14) Kojima, A.; Teshima, K.; Shirai, Y.; Miyasaka, T. Organometal Halide Perovskites as Visible-Light Sensitizers for Photovoltaic Cells. *Journal of the American Chemical Society* **2009**, *131*, 6050–6051.
- (15) Min, H.; Lee, D. Y.; Kim, J.; Kim, G.; Lee, K. S.; Kim, J.; Paik, M. J.; Kim, Y. K.; Kim, K. S.; Kim, M. G.; Shin, T. J.; Il Seok, S. Perovskite Solar Cells with Atomically Coherent Interlayers on SnO₂ Electrodes. *Nature* **2021**, *598*, 444–450.

- (16) Olivier-Fourcade, J.; Jumas, J. C.; Maurin, M.; Philippot, E. Mise en Évidence d'un Nouveau Sulfoiodure d'Étain et d'Antimoine $\text{Sn}_2\text{SbS}_2\text{I}_3$: Étude Structurale. *Zeitschrift für anorganische und allgemeine Chemie* **1980**, *468*, 91–98.
- (17) Nicolson, A.; Breternitz, J.; Kavanagh, S. R.; Tomm, Y.; Morita, K.; Squires, A. G.; Tovar, M.; Walsh, A.; Schorr, S.; Scanlon, D. O. Interplay of Static and Dynamic Disorder in the Mixed-Metal Chalcohalide $\text{Sn}_2\text{SbS}_2\text{I}_3$. *Journal of the American Chemical Society* **2023**, *145*, 12509–12517.
- (18) Ibanez, A.; Jumas, J.-C.; Olivier-Fourcade, J.; Philippot, E. Mise en évidence d'un désordre statistique dans les structures chalcogénoiodures d'étain et d'antimoine. *Journal of Solid State Chemistry* **1984**, *55*, 83–91.
- (19) Islam, S. M.; Malliakas, C. D.; Sarma, D.; Maloney, D. C.; Stoumpos, C. C.; Kontsevoi, O. Y.; Freeman, A. J.; Kanatzidis, M. G. Direct Gap Semiconductors $\text{Pb}_2\text{BiS}_2\text{I}_3$, $\text{Sn}_2\text{BiS}_2\text{I}_3$, and Sn_2BiSI_5 . *Chemistry of Materials* **2016**, *28*, 7332–7343.
- (20) Dolgikh, V. New Chalkogen-Halogenides of the Type $\text{M}_2\text{SbS}_2\text{I}_3$. *Izv. Akad. Nauk SSSR, Neorg. Mater.* **1985**, *21*, 1211–1214.
- (21) Doussier, C.; Moëlo, Y.; Léone, P.; Meerschaut, A.; Evain, M. Crystal Structure of $\text{pb}_2\text{SbS}_2\text{I}_3$, and Re-Examination of the Crystal Chemistry within the Group of (Pb/Sn/Sb) Chalcogeno-Iodides. *Solid State Sciences* **2007**, *9*, 792–803.
- (22) Roth, A. N.; Opare-Addo, J.; Gi, E.; Mena, S.; Guirado, G.; Schaller, R. D.; Smith, E. A.; Vela, J. Solution-Phase Synthesis and Photoluminescence of Quaternary Chalcohalide Semiconductors. *Chemistry of Materials* **2023**, *35*, 2165–2172.
- (23) Starosta, V. I.; Kroutil, J.; Beneš, L. Preparation and Fundamental Physical Properties of $\text{Sn}_2\text{SbS}_2\text{I}_3$ and $\text{Pb}_2\text{SbS}_2\text{I}_3$ Compounds. *Crystal Research and Technology* **1990**, *25*, 1439–1442.

- (24) Shockley, W.; Queisser, H. J. Detailed Balance Limit of Efficiency of P - n Junction Solar Cells. *Journal of Applied Physics* **1961**, *32*, 510–519.
- (25) Rühle, S. Tabulated Values of the Shockley–Queisser Limit for Single Junction Solar Cells. *Solar Energy* **2016**, *130*, 139–147.
- (26) Ganose, A. M.; Scanlon, D. O.; Walsh, A.; Hoyer, R. L. Z. The Defect Challenge of Wide-Bandgap Semiconductors for Photovoltaics and Beyond. *Nature Communications* **2022**, *13*, 4715.
- (27) Himanen, L.; Geurts, A.; Foster, A. S.; Rinke, P. Data-Driven Materials Science: Status, Challenges, and Perspectives. *Advanced Science* **2019**, *6*, 1900808.
- (28) Seidu, A.; Himanen, L.; Li, J.; Rinke, P. Database-Driven High-Throughput Study of Coating Materials for Hybrid Perovskites. *New Journal of Physics* **2019**, *21*, 083018.
- (29) Shapera, E. P.; Schleife, A. Database-Driven Materials Selection for Semiconductor Heterojunction Design. *Advanced Theory and Simulations* **2018**, *1*, 1800075.
- (30) Guo, J.; Clima, S.; Pourtois, G.; Van Houdt, J. Identifying Alternative Ferroelectric Materials beyond $\text{Hf}(\text{Zr})\text{O}_2$. *Applied Physics Letters* **2020**, *117*, 262903.
- (31) Schmidt, J.; Hoffmann, N.; Wang, H.-C.; Borlido, P.; M. A. Carrico, P. J.; F. T. Cerqueira, T.; Botti, S.; L. Marques, M. A. Large-Scale Machine-Learning-Assisted Exploration of the Whole Materials Space. *Materials Cloud Archive 2022.126* **2022-10-04**, doi: 10.24435/materialscloud:m7–50, accessed 2023–08–15.
- (32) Kim, K.; Ward, L.; He, J.; Krishna, A.; Agrawal, A.; Wolverton, C. Machine-Learning-Accelerated High-Throughput Materials Screening: Discovery of Novel Quaternary Heusler Compounds. *Physical Review Materials* **2018**, *2*, 123801.
- (33) Kulik, H. J. et al. Roadmap on Machine Learning in Electronic Structure. *Electronic Structure* **2022**, *4*, 023004.

- (34) Schmidt, J.; Marques, M. R. G.; Botti, S.; Marques, M. A. L. Recent Advances and Applications of Machine Learning in Solid-State Materials Science. *npj Computational Materials* **2019**, *5*, 83.
- (35) Ludwig, A. Discovery of new materials using combinatorial synthesis and high-throughput characterization of thin-film materials libraries combined with computational methods. *npj Computational Materials* **2019**, *5*, 70.
- (36) Stein, H. S.; Sanin, A.; Rahmanian, F.; Zhang, B.; Vogler, M.; Flowers, J. K.; Fischer, L.; Fuchs, S.; Choudhary, N.; Schroeder, L. From materials discovery to system optimization by integrating combinatorial electrochemistry and data science. *Current Opinion in Electrochemistry* **2022**, *35*, 101053.
- (37) Blum, V.; Gehrke, R.; Hanke, F.; Havu, P.; Havu, V.; Ren, X.; Reuter, K.; Scheffler, M. Ab Initio Molecular Simulations with Numeric Atom-Centered Orbitals. *Computer Physics Communications* **2009**, *180*, 2175–2196.
- (38) Havu, V.; Blum, V.; Havu, P.; Scheffler, M. Efficient Integration for All-Electron Electronic Structure Calculation Using Numeric Basis Functions. *Journal of Computational Physics* **2009**, *228*, 8367–8379.
- (39) Ren, X.; Rinke, P.; Blum, V.; Wieferink, J.; Tkatchenko, A.; Sanfilippo, A.; Reuter, K.; Scheffler, M. Resolution-of-Identity Approach to Hartree–Fock, Hybrid Density Functionals, RPA, MP2 and *GW* with Numeric Atom-Centered Orbital Basis Functions. *New Journal of Physics* **2012**, *14*, 053020.
- (40) Levchenko, S. V.; Ren, X.; Wieferink, J.; Johanni, R.; Rinke, P.; Blum, V.; Scheffler, M. Hybrid Functionals for Large Periodic Systems in an All-Electron, Numeric Atom-Centered Basis Framework. *Computer Physics Communications* **2015**, *192*, 60–69.
- (41) Yu, V. W.-z.; Corsetti, F.; García, A.; Huhn, W. P.; Jacquelin, M.; Jia, W.; Lange, B.; Lin, L.; Lu, J.; Mi, W.; Seifitokaldani, A.; Vázquez-Mayagoitia, Á.; Yang, C.; Yang, H.;

- Blum, V. ELSI: A Unified Software Interface for Kohn–Sham Electronic Structure Solvers. *Computer Physics Communications* **2018**, *222*, 267–285.
- (42) Ihrig, A. C.; Wieferink, J.; Zhang, I. Y.; Ropo, M.; Ren, X.; Rinke, P.; Scheffler, M.; Blum, V. Accurate Localized Resolution of Identity Approach for Linear-Scaling Hybrid Density Functionals and for Many-Body Perturbation Theory. *New Journal of Physics* **2015**, *17*, 093020.
- (43) Perdew, J. P.; Ruzsinszky, A.; Csonka, G. I.; Vydrov, O. A.; Scuseria, G. E.; Constantin, L. A.; Zhou, X.; Burke, K. Restoring the Density-Gradient Expansion for Exchange in Solids and Surfaces. *Physical Review Letters* **2008**, *100*, 136406.
- (44) Perdew, J. P.; Ruzsinszky, A.; Csonka, G. I.; Vydrov, O. A.; Scuseria, G. E.; Constantin, L. A.; Zhou, X.; Burke, K. Erratum: Restoring the Density-Gradient Expansion for Exchange in Solids and Surfaces [Phys. Rev. Lett. **100** , 136406 (2008)]. *Physical Review Letters* **2009**, *102*, 039902.
- (45) Yang, R. X.; Skelton, J. M.; da Silva, E. L.; Frost, J. M.; Walsh, A. Spontaneous Octahedral Tilting in the Cubic Inorganic Cesium Halide Perovskites CsSnX₃ and CsPbX₃ (X = F, Cl, Br, I). *The Journal of Physical Chemistry Letters* **2017**, *8*, 4720–4726.
- (46) Bokdam, M.; Lahnsteiner, J.; Ramberger, B.; Schäfer, T.; Kresse, G. Assessing Density Functionals Using Many Body Theory for Hybrid Perovskites. *Physical Review Letters* **2017**, *119*, 145501.
- (47) Li, J.; Pan, F.; Zhang, G.-X.; Liu, Z.; Dong, H.; Wang, D.; Jiang, Z.; Ren, W.; Ye, Z.-G.; Todorović, M.; Rinke, P. Structural Disorder by Octahedral Tilting in Inorganic Halide Perovskites: New Insight with Bayesian Optimization. *arXiv:2303.08426 [cond-mat.mtrl-sci]* **2023-03-15**, doi: 10.48550/arXiv.2303.08426, accessed 2023-08-15.
- (48) Knuth, F.; Carbogno, C.; Atalla, V.; Blum, V.; Scheffler, M. All-Electron Formalism

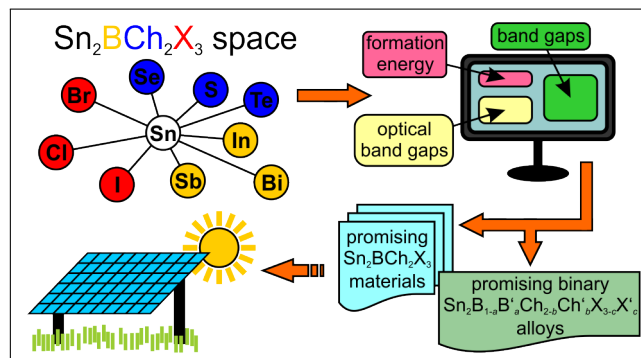
- for Total Energy Strain Derivatives and Stress Tensor Components for Numeric Atom-Centered Orbitals. *Computer Physics Communications* **2015**, *190*, 33–50.
- (49) van Lenthe, E.; Baerends, E. J.; Snijders, J. G. Relativistic Regular Two-component Hamiltonians. *The Journal of Chemical Physics* **1993**, *99*, 4597–4610.
- (50) Heyd, J.; Scuseria, G. E.; Ernzerhof, M. Hybrid Functionals Based on a Screened Coulomb Potential. *The Journal of Chemical Physics* **2003**, *118*, 8207–8215.
- (51) Heyd, J.; Scuseria, G. E.; Ernzerhof, M. Erratum: “Hybrid Functionals Based on a Screened Coulomb Potential” [J. Chem. Phys. 118, 8207 (2003)]. *The Journal of Chemical Physics* **2006**, *124*, 219906.
- (52) Krukau, A. V.; Vydrov, O. A.; Izmaylov, A. F.; Scuseria, G. E. Influence of the Exchange Screening Parameter on the Performance of Screened Hybrid Functionals. *The Journal of Chemical Physics* **2006**, *125*, 224106.
- (53) Huhn, W. P.; Blum, V. One-Hundred-Three Compound Band-Structure Benchmark of Post-Self-Consistent Spin-Orbit Coupling Treatments in Density Functional Theory. *Physical Review Materials* **2017**, *1*, 033803.
- (54) Ambrosch-Draxl, C.; Sofo, J. O. Linear Optical Properties of Solids within the Full-Potential Linearized Augmented Planewave Method. *Computer Physics Communications* **2006**, *175*, 1–14.
- (55) Van de Walle, C. G.; Neugebauer, J. Structure and Energetics of Nitride Surfaces under MOCVD Growth Conditions. *Journal of Crystal Growth* **2003**, *248*, 8–13.
- (56) Jain, A.; Ong, S. P.; Hautier, G.; Chen, W.; Richards, W. D.; Dacek, S.; Cholia, S.; Gunter, D.; Skinner, D.; Ceder, G.; Persson, K. A. Commentary: The Materials Project: A Materials Genome Approach to Accelerating Materials Innovation. *APL Materials* **2013**, *1*, 011002.

- (57) Momma, K.; Izumi, F. *VESTA* : A Three-Dimensional Visualization System for Electronic and Structural Analysis. *Journal of Applied Crystallography* **2008**, *41*, 653–658.
- (58) Sutherland, B. R. Solar Materials Find Their Band Gap. *Joule* **2020**, *4*, 984–985.
- (59) Evans, M.; Andersen, C.; Dwaraknath, S.; Scheidgen, M.; Fekete, Á.; Winston, D. Optimade-Python-Tools: A Python Library for Serving and Consuming Materials Data via OPTIMADE APIs. *Journal of Open Source Software* **2021**, *6*, 3458.
- (60) Andersen, C. W. et al. OPTIMADE, an API for Exchanging Materials Data. *Scientific Data* **2021**, *8*, 217.
- (61) Curtarolo, S.; Setyawan, W.; Wang, S.; Xue, J.; Yang, K.; Taylor, R. H.; Nelson, L. J.; Hart, G. L.; Sanvito, S.; Buongiorno-Nardelli, M.; Mingo, N.; Levy, O. AFLOWLIB.ORG: A Distributed Materials Properties Repository from High-Throughput Ab Initio Calculations. *Computational Materials Science* **2012**, *58*, 227–235.
- (62) Toher, C. et al. In *Handbook of Materials Modeling*; Andreoni, W., Yip, S., Eds.; Springer International Publishing: Cham, 2018; pp 1–28.
- (63) Gražulis, S.; Chateigner, D.; Downs, R. T.; Yokochi, A. F. T.; Quirós, M.; Lutterotti, L.; Manakova, E.; Butkus, J.; Moeck, P.; Le Bail, A. Crystallography Open Database – an Open-Access Collection of Crystal Structures. *Journal of Applied Crystallography* **2009**, *42*, 726–729.
- (64) Gražulis, S.; Daškevič, A.; Merkys, A.; Chateigner, D.; Lutterotti, L.; Quirós, M.; Serebryanaya, N. R.; Moeck, P.; Downs, R. T.; Le Bail, A. Crystallography Open Database (COD): An Open-Access Collection of Crystal Structures and Platform for World-Wide Collaboration. *Nucleic Acids Research* **2012**, *40*, D420–D427.

- (65) Groom, C. R.; Bruno, I. J.; Lightfoot, M. P.; Ward, S. C. The Cambridge Structural Database. *Acta Crystallographica Section B Structural Science, Crystal Engineering and Materials* **2016**, *72*, 171–179.
- (66) Bergerhoff, G.; Brown, I. D.; Allen, F. H. *Crystallographic Databases*; International Union of Crystallography: Chester, 1987; pp 77–95.
- (67) Zagorac, D.; Müller, H.; Ruehl, S.; Zagorac, J.; Rehme, S. Recent Developments in the Inorganic Crystal Structure Database: Theoretical Crystal Structure Data and Related Features. *Journal of Applied Crystallography* **2019**, *52*, 918–925.
- (68) Allmann, R.; Hinek, R. The Introduction of Structure Types into the Inorganic Crystal Structure Database ICSD. *Acta Crystallographica Section A Foundations of Crystallography* **2007**, *63*, 412–417.
- (69) Belsky, A.; Hellenbrandt, M.; Karen, V. L.; Luksch, P. New Developments in the Inorganic Crystal Structure Database (ICSD): Accessibility in Support of Materials Research and Design. *Acta Crystallographica Section B Structural Science* **2002**, *58*, 364–369.
- (70) Choudhary, K. et al. The Joint Automated Repository for Various Integrated Simulations (JARVIS) for Data-Driven Materials Design. *npj Computational Materials* **2020**, *6*, 173.
- (71) Talirz, L. et al. Materials Cloud, a Platform for Open Computational Science. *Scientific Data* **2020**, *7*, 299.
- (72) Pizzi, G.; Cepellotti, A.; Sabatini, R.; Marzari, N.; Kozinsky, B. AiiDA: Automated Interactive Infrastructure and Database for Computational Science. *Computational Materials Science* **2016**, *111*, 218–230.

- (73) Huber, S. P. et al. AiiDA 1.0, a Scalable Computational Infrastructure for Automated Reproducible Workflows and Data Provenance. *Scientific Data* **2020**, *7*, 300.
- (74) Draxl, C.; Scheffler, M. NOMAD: The FAIR Concept for Big Data-Driven Materials Science. *MRS Bulletin* **2018**, *43*, 676–682.
- (75) Ghiringhelli, L. M.; Carbogno, C.; Levchenko, S.; Mohamed, F.; Huhs, G.; Lüders, M.; Oliveira, M.; Scheffler, M. Towards Efficient Data Exchange and Sharing for Big-Data Driven Materials Science: Metadata and Data Formats. *npj Computational Materials* **2017**, *3*, 46.
- (76) Evans, M.; Morris, A. Matador: A Python Library for Analysing, Curating and Performing High-Throughput Density-Functional Theory Calculations. *Journal of Open Source Software* **2020**, *5*, 2563.
- (77) Armiento, R. In *Machine Learning Meets Quantum Physics*; Schütt, K. T., Chmiela, S., von Lilienfeld, O. A., Tkatchenko, A., Tsuda, K., Müller, K.-R., Eds.; Springer International Publishing: Cham, 2020; Vol. 968; pp 377–395.
- (78) Saal, J. E.; Kirklin, S.; Aykol, M.; Meredig, B.; Wolverton, C. Materials Design and Discovery with High-Throughput Density Functional Theory: The Open Quantum Materials Database (OQMD). *JOM* **2013**, *65*, 1501–1509.
- (79) Merkys, A.; Mounet, N.; Cepellotti, A.; Marzari, N.; Gražulis, S.; Pizzi, G. A Posteriori Metadata from Automated Provenance Tracking: Integration of AiiDA and TCO. *Journal of Cheminformatics* **2017**, *9*, 56.
- (80) Zhou, J.; Shen, L.; Costa, M. D.; Persson, K. A.; Ong, S. P.; Huck, P.; Lu, Y.; Ma, X.; Chen, Y.; Tang, H.; Feng, Y. P. 2DMatPedia, an Open Computational Database of Two-Dimensional Materials from Top-down and Bottom-up Approaches. *Scientific Data* **2019**, *6*, 86.

TOC Graphic



Screening Mixed-Metal $\text{Sn}_2\text{M(III)Ch}_2\text{X}_3$ Chalcohalides for Photovoltaic Applications

Pascal Henkel,[†] Jingrui Li,[‡] G. Krishnamurthy Grandhi,[¶] Paola Vivo,[¶] and Patrick
Rinke^{*,†}

[†]*Department of Applied Physics, Aalto University, P.O.Box 11100, FI-00076 AALTO,
Finland*

[‡]*Electronic Materials Research Laboratory, Key Laboratory of the Ministry of Education
and International Center for Dielectric Research, School of Electronic Science and
Engineering & International Joint Laboratory for Micro/Nano Manufacturing and
Measurement Technology, Xi'an Jiaotong University, Xi'an 710049, China*

[¶]*Hybrid Solar Cells, Faculty of Engineering and Natural Sciences, Tampere University,
P.O. Box 541, Tampere, FI, 33014, Finland*

E-mail: patrick.rinke@aalto.fi

S1: Band structure of $\text{Sn}_2\text{InS}_2\text{Br}_3$

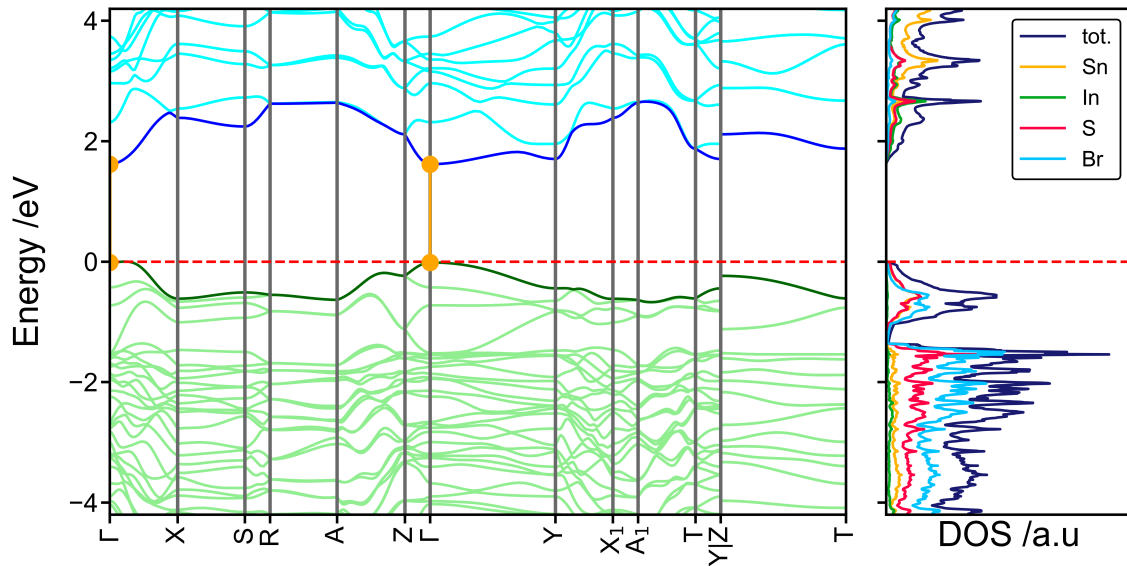


Figure 1: Bandstructure (left) and normalized density of states (right) for $\text{Sn}_2\text{InS}_2\text{Br}_3$ for the $Cmcm$ space group. Conduction bands are shown in green and valence bands in blue. The total and partial density of state per element are provided.

S2: Lattice parameters, formation energies, fundamental and optical band gaps for $\text{Sn}_2\text{M(III)Ch}_2\text{X}_3$ materials

Table 1: Summary of the calculated lattice parameters (a , b , c , a/c -ratio), as well as the formation energy E_{form} (related to the i -th elements) using PBEsol level of theory and the fundamental lowest direct band gap $E_{\text{g, dir.}}$, and for indirect $\text{Sn}_2\text{M(III)Ch}_2\text{X}_3$ materials also the lowest indirect band gap ($E_{\text{g, ind.}}$), as well as the optical band gap using HSE06+SOC level of theory. -/- marks that either the material has no indirect/no band gap at all or that no experimental values are available. $\text{Sn}_2\text{M(III)Ch}_2\text{X}_3$ materials highlighted orange (direct) or gray (indirect) if their fundamental band gap is within the range of 0.7 eV to 2.0 eV.

System	Group	lat. parameters				$E_{\text{form}} / \text{eV Atom}^{-1}$	$E_{\text{g, dir.}}$	$E_{\text{g, ind.}} / \text{eV}$	$E_{\text{g, opt.}} / \text{eV}$
		$a / \text{\AA}$	$b / \text{\AA}$	$c / \text{\AA}$	c/a				
$\text{Sn}_2\text{InS}_2\text{Cl}_3$	<i>Cmcm</i>	4.23	14.12	14.3	3.38	-726	1.305	1.251	1.49
	<i>Cmc2₁</i>	3.94	14.22	15.0	3.81	-772	1.834	1.692	1.89
	<i>P2₁/c</i>	6.27	16.19	7.88	1.26	-779	2.433	2.037	2.440
$\text{Sn}_2\text{InS}_2\text{Br}_3$	<i>Cmcm</i>	4.22	14.80	14.50	3.44	-650	1.617	-/-	1.977
	<i>Cmc2₁</i>	4.11	15.16	15.53	3.77	-693	1.742	-/-	1.783
	<i>P2₁/c</i>	6.36	16.55	8.07	1.27	-690	1.985	1.616	1.996
$\text{Sn}_2\text{InS}_2\text{I}_3$	<i>Cmcm</i>	4.37	15.68	14.83	3.40	-520	1.395	-/-	1.934
	<i>Cmc2₁</i>	4.06	14.13	19.25	4.75	-519	1.120	0.598	1.187
	<i>P2₁/c</i>	7.66	16.56	8.41	1.1	-565	2.278	2.102	2.313
$\text{Sn}_2\text{InSe}_2\text{Cl}_3$	<i>Cmcm</i>	4.13	14.94	14.9	3.60	-718	0.661	0.597	0.675
	<i>Cmc2₁</i>	4.08	14.09	16.02	3.93	-767	1.046	-/-	1.684
	<i>P2₁/c</i>	6.35	16.79	8.09	1.27	-765	2.076	1.925	2.088
$\text{Sn}_2\text{InSe}_2\text{Br}_3$	<i>Cmcm</i>	4.42	14.54	15.01	3.40	-651	1.105	-/-	1.477
	<i>Cmc2₁</i>	3.98	15.22	15.58	3.91	-699	1.373	1.338	1.396
	<i>P2₁/c</i>	6.41	17.09	8.23	1.28	-688	1.843	1.488	1.855
$\text{Sn}_2\text{InSe}_2\text{I}_3$	<i>Cmcm</i>	4.39	15.73	15.31	3.49	-534	1.369	1.299	1.397
	<i>Cmc2₁</i>	4.32	15.93	16.32	3.78	-577	0.677	-/-	1.282
	<i>P2₁/c</i>	7.41	17.62	8.5	1.15	-567	1.947	1.785	1.960
$\text{Sn}_2\text{InTe}_2\text{Cl}_3$	<i>Cmcm</i>	4.19	12.25	18.4	4.39	-542	0.558	0.455	0.651
	<i>Cmc2₁</i>	4.16	13.24	17.21	4.13	-639	0.915	0.804	1.011
	<i>P2₁/c</i>	6.53	17.82	8.58	1.32	-610	1.594	-/-	1.713
$\text{Sn}_2\text{InTe}_2\text{Br}_3$	<i>Cmcm</i>	4.28	12.34	18.41	4.30	-488	-/-	-/-	-/-
	<i>Cmc2₁</i>	4.31	14.70	16.90	3.92	-559	0.531	-/-	0.786
	<i>P2₁/c</i>	6.48	18.04	8.60	1.33	-543	1.461	-/-	1.592
$\text{Sn}_2\text{InTe}_2\text{I}_3$	<i>Cmcm</i>	4.56	15.6	16.26	3.57	-425	1.089	0.994	1.126
	<i>Cmc2₁</i>	4.3	15.34	16.92	3.94	-460	0.867	0.802	0.964
	<i>P2₁/c</i>	6.58	18.87	8.74	1.33	-438	1.109	1.083	1.201
$\text{Sn}_2\text{SbS}_2\text{Cl}_3$	<i>Cmcm</i>	4.08	12.63	15.88	3.89	-649	1.679	1.611	1.773
	<i>Cmc2₁</i>	4.01	13.81	16.0	3.99	-655	1.242	1.056	1.288
	<i>P2₁/c</i>	6.96	16.05	8.08	1.16	-702	2.451	2.170	2.477
$\text{Sn}_2\text{SbS}_2\text{Br}_3$	<i>Cmcm</i>	4.1	13.47	15.4	3.76	-574	1.474	0.883	1.527
	<i>Cmc2₁</i>	4.1	13.92	16.12	3.93	-592	1.248	1.055	1.344
	<i>P2₁/c</i>	7.01	16.06	8.19	1.17	-646	2.194	1.989	2.294
$\text{Sn}_2\text{SbS}_2\text{I}_3$	<i>Cmcm</i>	4.24	13.84	15.76	3.72	-486	0.997	0.947	1.547
	<i>Cmc2₁</i>	4.26	14.22	16.24	3.81	-497	1.007	-/-	1.506
	<i>P2₁/c</i>	7.25	16.24	8.47	1.17	-555	1.762	1.686	1.771
	Exp. ^a	4.25	13.99	16.38	3.85	-/-	-/-	-/-	1.41
$\text{Sn}_2\text{SbSe}_2\text{Cl}_3$	<i>Cmcm</i>	4.16	12.48	16.92	4.07	-646	1.411	-/-	1.816
	<i>Cmc2₁</i>	4.07	14.01	16.45	4.04	-651	1.002	-/-	1.261
	<i>P2₁/c</i>	7.06	17.98	8.06	1.14	-692	2.181	1.839	2.202

System	Group	lat. parameters				$E_{\text{form}} / \text{eV Atom}^{-1}$	$E_{\text{g, dir.}}$	$E_{\text{g, ind.}} / \text{eV}$	$E_{\text{g, opt.}} / \text{eV}$
		$a / \text{\AA}$	$b / \text{\AA}$	$c / \text{\AA}$	c/a				
Sn ₂ SbSe ₂ Br ₃	<i>Cmcm</i>	4.13	12.94	17.75	4.3	-572	1.412	1.330	1.504
	<i>Cmc2₁</i>	4.16	14.22	16.73	4.03	-586	0.941	0.891	1.044
	<i>P2₁/c</i>	7.1	17.16	8.29	1.17	-631	2.028	1.642	2.100
Sn ₂ SbSe ₂ I ₃	<i>Cmcm</i>	4.28	13.95	16.44	3.84	-473	1.057	0.800	1.056
	<i>Cmc2₁</i>	4.31	14.50	16.91	3.93	-493	0.962	-/-	1.640
	<i>P2₁/c</i>	7.28	17.08	8.57	1.18	-547	1.892	1.672	1.983
	Exp. ^b	4.30	14.09	17.22	4.01	-/-	-/-	-/-	-/-
Sn ₂ SbTe ₂ Cl ₃	<i>Cmcm</i>	4.34	12.40	17.68	4.07	-530	0.943	0.874	0.997
	<i>Cmc2₁</i>	4.34	12.39	17.70	4.08	-523	0.950	-/-	1.370
	<i>P2₁/c</i>	6.45	18.1	8.36	1.30	-588	0.559	0.480	0.653
Sn ₂ SbTe ₂ Br ₃	<i>Cmcm</i>	4.24	12.51	19.69	4.64	-456	0.699	0.490	0.763
	<i>Cmc2₁</i>	4.27	14.66	17.39	4.07	-456	1.027	0.980	1.063
	<i>P2₁/c</i>	6.59	18.5	8.42	1.28	-518	0.545	0.245	0.567
Sn ₂ SbTe ₂ I ₃	<i>Cmcm</i>	4.34	13.57	19.47	4.48	-353	0.786	0.465	0.795
	<i>Cmc2₁</i>	4.28	14.31	18.73	4.37	-358	0.376	0.186	0.433
	<i>P2₁/c</i>	7.02	18.82	8.67	1.24	-412	0.852	0.021	1.255
Sn ₂ BiS ₂ Cl ₃	<i>Cmcm</i>	3.99	13.91	16.02	4.02	-714	1.535	0.986	1.548
	<i>Cmc2₁</i>	4.07	13.72	15.98	3.93	-716	1.146	1.034	1.169
	<i>P2₁/c</i>	6.97	15.93	8.1	1.16	-732	2.187	1.84	2.191
Sn ₂ BiS ₂ Br ₃	<i>Cmcm</i>	4.11	13.42	15.68	3.81	-650	1.343	0.956	1.434
	<i>Cmc2₁</i>	4.11	13.42	15.68	3.82	-651	1.405	1.124	1.504
	<i>P2₁/c</i>	7.03	16.04	8.23	1.17	-675	1.968	1.717	2.065
Sn ₂ BiS ₂ I ₃	<i>Cmcm</i>	4.26	13.92	15.93	3.74	-552	0.988	-/-	1.390
	<i>Cmc2₁</i>	4.26	13.92	15.94	3.74	-553	1.013	-/-	1.420
	<i>P2₁/c</i>	7.3	16.23	8.52	1.17	-583	1.606	1.490	1.599
	Exp. ^c	4.29	14.12	16.41	3.83	-/-	-/-	-/-	1.22
Sn ₂ BiSe ₂ Cl ₃	<i>Cmcm</i>	4.03	12.5	17.07	4.23	-713	1.104	1.096	1.124
	<i>Cmc2₁</i>	4.13	13.98	16.46	3.99	-708	0.902	0.714	0.952
	<i>P2₁/c</i>	6.41	17.23	8.22	1.28	-731	1.196	1.076	1.254
Sn ₂ BiSe ₂ Br ₃	<i>Cmcm</i>	4.13	13.02	17.29	4.19	-635	0.965	0.666	1.063
	<i>Cmc2₁</i>	4.21	14.14	16.74	3.98	-642	0.841	0.827	0.853
	<i>P2₁/c</i>	6.9	17.19	8.33	1.21	-662	1.425	1.118	1.452
Sn ₂ BiSe ₂ I ₃	<i>Cmcm</i>	4.31	13.99	16.62	3.86	-538	1.048	0.769	1.141
	<i>Cmc2₁</i>	4.35	14.47	16.87	3.87	-538	1.064	0.881	1.162
	<i>P2₁/c</i>	7.33	17.08	8.6	1.17	-575	1.66	1.474	1.751
Sn ₂ BiTe ₂ Cl ₃	<i>Cmcm</i>	4.15	12.37	17.83	4.30	-580	0.738	-/-	1.079
	<i>Cmc2₁</i>	4.20	12.37	17.84	4.25	-579	0.764	0.697	0.863
	<i>P2₁/c</i>	6.53	18.02	8.48	1.30	-612	0.498	0.476	0.579
Sn ₂ BiTe ₂ Br ₃	<i>Cmcm</i>	4.24	12.63	18.26	4.31	-510	0.852	0.715	0.854
	<i>Cmc2₁</i>	4.24	12.64	18.27	4.31	-510	0.854	0.718	0.856
	<i>P2₁/c</i>	6.68	18.39	8.53	1.28	-542	0.597	0.440	0.692
Sn ₂ BiTe ₂ I ₃	<i>Cmcm</i>	4.38	13.30	18.73	4.28	-399	-/-	-/-	-/-
	<i>Cmc2₁</i>	4.48	14.90	17.96	4.05	-407	0.610	0.582	0.692
	<i>P2₁/c</i>	7.12	18.67	8.75	1.23	-439	0.890	0.256	0.931

^a Lat. para. are taken from RT ($T = 293$ K) XRD meas. using MoK α radiation¹ and band gap are taken from UV/vis absorption meas.²

^b Lat. para. are taken from low-temp. ($T = 173$ K) XRD meas. using MoK α radiation.¹

^c Lat. para. are taken from RT ($T = 293$ K) XRD meas. using MoK α radiation and band gap are taken from UV/vis absorption meas.³

S3: Formation energies for indirect $\text{Sn}_2\text{M(III)Ch}_2\text{X}_3$ materials

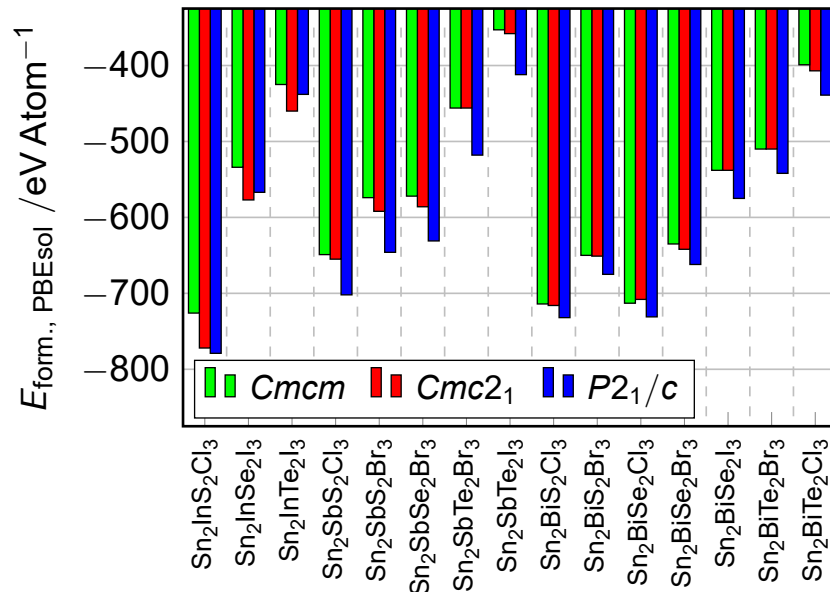


Figure 2: Formation energy (calculated with PBEsol) of the 15 indirect $\text{Sn}_2\text{M(III)Ch}_2\text{X}_3$ compounds of interest for $Cmcm$ (green), $Cmc2_1$ (red) and $P2_1/c$ (blue) space groups.

S4: Band gaps for all identified direct and indirect $\text{Sn}_2\text{M(III)Ch}_2\text{X}_3$ materials

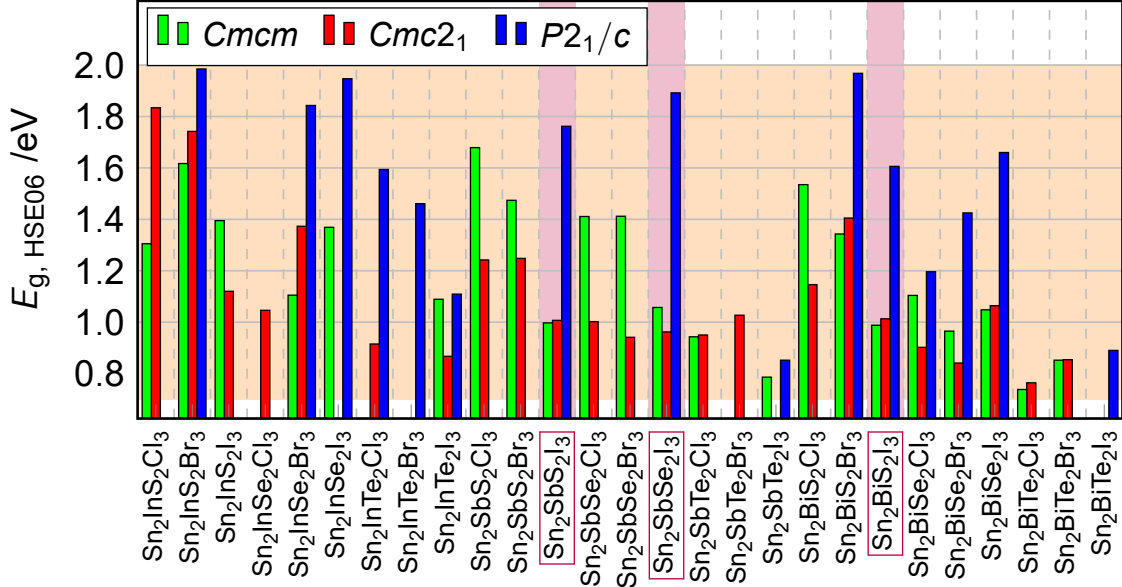


Figure 3: Direct band gaps (HSE06+SOC level of theory) for 12 $\text{Sn}_2\text{SbS}_2\text{I}_3$ materials of interest and energetically lowest direct band gaps (HSE06+SOC level of theory) for 15 indirect $\text{Sn}_2\text{SbS}_2\text{I}_3$ materials of interest for $Cmcm$ (green), $Cmc2_1$ (red) and $P2_1/c$ (blue) space groups. Three structures - $\text{Sn}_2\text{SbS}_2\text{I}_3$,⁴ $\text{Sn}_2\text{SbSe}_2\text{I}_3$,¹ and $\text{Sn}_2\text{BiS}_2\text{I}_3$ ³ - that are already known from the literature, are highlighted in purple.

S5: $\text{Sn}_2\text{M(III)}_{1-a}\text{M(III)}'_a\text{Ch}_{2-b}\text{Ch}'_b\text{X}_{3-c}\text{X}'_c$ alloy compounds based on direct and indirect $\text{Sn}_2\text{M(III)Ch}_2\text{X}_3$ materials

Similar to the described approach of $\text{Sn}_2\text{M(III)}_{1-a}\text{M(III)}'_a\text{Ch}_{2-b}\text{Ch}'_b\text{X}_{3-c}\text{X}'_c$ alloys with only $\text{Sn}_2\text{M(III)Ch}_2\text{X}_3$ materials with direct gaps, we now consider also $\text{Sn}_2\text{M(III)Ch}_2\text{X}_3$ materials with an indirect gaps. In this way, we obtain a considerably larger $\text{Sn}_2\text{M(III)}_{1-a}\text{M(III)}'_a\text{Ch}_{2-b}\text{Ch}'_b\text{X}_{3-c}\text{X}'_c$ material space. The alloys we consider are composed either of two direct $\text{Sn}_2\text{M(III)Ch}_2\text{X}_3$ materials, or of one direct and one indirect material, as well as of two indirect materials. For the indirect $\text{Sn}_2\text{M(III)Ch}_2\text{X}_3$ compounds, we use the energetically lowest direct band gap, analogous to fig. 3 in the SI. By this we can identify a total of 81 $\text{Sn}_2\text{M(III)}_{1-a}\text{M(III)}'_a\text{Ch}_{2-b}\text{Ch}'_b\text{X}_{3-c}\text{X}'_c$ alloys [see fig. 4 in the SI], 69 of which are composed of at least one indirect $\text{Sn}_2\text{M(III)Ch}_2\text{X}_3$ material.

The $P2_1/c$ space group is no longer underrepresented and a homogenous distribution of the three space groups is obtained. Similar to their direct counterparts, the alloys within the $Cmcm$ and $Cmc2_1$ space group tend to have band gaps in the lower part of the spectra (about 1 eV), whereas $P2_1/c$ alloys tend towards the upper region of the spectra (about 2 eV). These compounds open up the $\text{Sn}_2\text{M(III)}_{1-a}\text{M(III)}'_a\text{Ch}_{2-b}\text{Ch}'_b\text{X}_{3-c}\text{X}'_c$ space and can also be considered for future band gap tuning. Thus, we assume that at least a part of compositions within this $\text{Sn}_2\text{M(III)}_{1-a}\text{M(III)}'_a\text{Ch}_{2-b}\text{Ch}'_b\text{X}_{3-c}\text{X}'_c$ space may have a direct band gap that fulfils our materials design criterion, whereby these alloys might also be of interest.

References

- (1) Ibanez, A.; Jumas, J.-C.; Olivier-Fourcade, J.; Philippot, E. Mise en évidence d'un désordre statistique dans les structures chalcogénoiodures d'étain et d'antimoine. *Journal of Solid State Chemistry* **1984**, *55*, 83–91.
- (2) Nie, R.; Lee, K. S.; Hu, M.; Paik, M. J.; Seok, S. I. Heteroleptic Tin-Antimony Sulfoiodide for Stable and Lead-free Solar Cells. *Matter* **2020**, *3*, 1701–1713.
- (3) Islam, S. M.; Malliakas, C. D.; Sarma, D.; Maloney, D. C.; Stoumpos, C. C.; Kontsevoi, O. Y.; Freeman, A. J.; Kanatzidis, M. G. Direct Gap Semiconductors $\text{Pb}_2\text{BiS}_2\text{I}_3$, $\text{Sn}_2\text{BiS}_2\text{I}_3$, and Sn_2BiSI_5 . *Chemistry of Materials* **2016**, *28*, 7332–7343.
- (4) Olivier-Fourcade, J.; Jumas, J. C.; Maurin, M.; Philippot, E. Mise en Évidence d'un Nouveau Sulfoiodure d'Étain et d'Antimoine $\text{Sn}_2\text{SbS}_2\text{I}_3$: Étude Structurale. *Zeitschrift für anorganische und allgemeine Chemie* **1980**, *468*, 91–98.